Local and Nanoscale Structure and Speciation in the PuO$_{2+x-y}$(OH)$_{2y}$·zH$_2$O System

Steven D. Conradson,*,† Bruce D. Begg,‡ David L. Clark,† Christophe den Auwer,§
Mei Ding,† Peter K. Dorhout,⊥ Francisco J. Espinosa-Faller,†,∥ Pamela L. Gordon,†
Richard G. Haire,# Nancy J. Hess,∇ Ryan F. Hess,† D. Webster Keogh,†
Luis A. Morales,† Mary P. Neu,† Patricia Paviet-Hartmann,† Wolfgang Runde,†
C. Drew Tait,† D. Kirk Veirs,† and Phillip M. Villella†

*Contribution from the Los Alamos National Laboratory, Los Alamos, New Mexico 87545,
Australian Nuclear Science and Technology Organisation, Menai NSW 2234, Australia,
Commissariat a l'Energie Atomique Marcoule, 30207 Bagnols sur Ceze Cedex, France,
Colorado State University, Fort Collins, Colorado 80523, Centro Marista de
Estudios Superiores, Merida, Yucatan, Mexico, Oak Ridge National Laboratory,
Oak Ridge, Tennessee 37831, and Pacific Northwest National Laboratory,
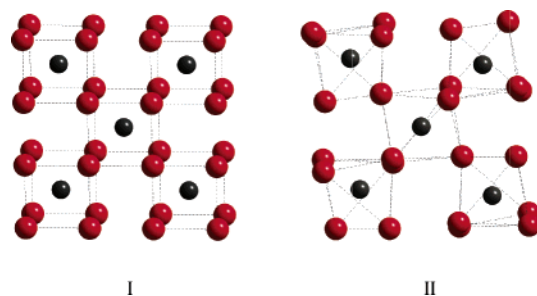Richland, Washington 99352*

Received February 13, 2004; E-mail: conradson@lanl.gov

Abstract: Pu L$_3$ X-ray absorption fine structure spectra from 24 samples of PuO$_{2+x}$ (and two related Pu-substituted oxides), prepared by a variety of methods, demonstrate that (1) although the Pu sublattice remains the ordered part of the Pu distribution, the nearest-neighbor O atoms even at $x = 0$ are found in a multisite distribution with Pu−O distances consistent with the stable incorporation of OH$^-$ (and possibly H$_2$O and H$^+$) into the PuO$_2$ lattice; (2) the excess O from oxidation is found at Pu−O distances <1.9 Å, consistent with the multiply bound "oxo"-type ligands found in molecular complexes of Pu(V) and Pu(VI); (3) the Pu associated with these oxo groups is most likely Pu(V), so that the excess O probably occurs as PuO$_2^+$ moieties that are aperiodically distributed through the lattice; and (4) the collective interactions between these defect sites most likely cause them to cluster so as give nanoscale heterogeneity in the form of domains that may have unusual reactivity, observed as sequential oxidation by H$_2$O at ambient conditions. The most accurate description of PuO$_2$ is therefore actually PuO$_{2+x-y}$(OH)$_{2y}$·zH$_2$O, with pure, ordered, homogeneous PuO$_2$ attained only when H$_2$O is rigorously excluded and the O activity is relatively low.

Introduction

The phase equilibria of plutonium oxides are quite complex.[1−3] In the *Fm3m* fluorite-type structure of PuO$_2$, the Pu sublattice is also fcc, and within this framework of the cations there are tetrahedral (*t*) and octahedral (*o*) interstices that may be occupied by the O atoms. In PuO$_2$, all the O atoms are in tetrahedral sites and the octahedral sites are vacant, with the Pu atoms centered in alternating cubes of O atoms (**I**).[4] Intriguingly, the cubic sesquioxide Pu$_2$O$_3$ structure is related to the fluorite PuO$_2$ structure by leaving the Pu sublattice almost unchanged while removing every fourth O atom, so that the PuO$_8$ cubes become two types of PuO$_6$ octahedra (**II**).[3,4] The oxidation of Pu$_2$O$_3$ to PuO$_2$ is analogous to UO$_{2+x}$, continuous with some distinct intermediates and retention of the An sublattice.

I   II

Since the oxo complexes of higher valent actinides have higher aqueous solubilities than PuO$_2$, the identification of PuO$_{2+x}$ was especially significant vis-à-vis Pu environmental chemistry. Transport models for Pu contamination have assumed that the solubility is that of PuO$_2$, which is a thermodynamic minimum near neutral pH in equilibrium with air and H$_2$O.[5]

† Los Alamos National Laboratory.
‡ ANSTO.
§ CEA Marcoule.
⊥ Colorado State University.
∥ Centro Marista de Estudios Superiores.
Oak Ridge National Laboratory.
∇ Pacific Northwest National Laboratory.
(1) Wriedt, H. A. *Bull. Alloy Phase Diagrams* **1990**, *11*, 184.
(2) Haschke, J. M.; Haire, R. G. *Advances in Plutonium Chemistry 1967−2000*; The American Nuclear Society: La Grange Park, IL, 2000.
(3) Haschke, J. M.; Allen, T. H.; Morales, L. A. *Science* **2000**, *287*, 285.
(4) Haschke, J. M.; Allen, T. H.; Morales, L. A. Challenges in Plutonium Science. In *Los Alamos Science*; Cooper, N. G., Schecker, J. A., Eds.; Los Alamos National Laboratory: Los Alamos, NM, 2000; Vol. 26, p 252.

The existence of a related species that would have been formed in many routine Pu processing operations in which some of the Pu was more soluble and would be leached out on contact with H_2O could significantly increase the hazard of Pu-contaminated soils. This type of speciation and behavior would also have significant effects on Pu storage and disposal as well as other technologically important phenomena, such as corrosion.[6] Identification of the Pu speciation in PuO_{2+x}, as well as any anomalous reactivities resulting from the excess O atoms, is therefore not only an interesting scientific problem relevant to the general issue of structure−function relationships in transition metal oxides but is also critical with respect to these more global concerns.

A large body of work, both prior to and following this seminal paper,[3] has attempted to expand on some of the structural, chemical, and thermodynamic characteristics of PuO_{2+x}.[7−10] These reports, however, are predicated on a homogeneous model for this system and do not include hydrolytic, non-oxidative additions of H_2O that may greatly increase its complexity.[11,12] This has resulted in modeling using the incorrect placement of the extra O atoms at interstitial sites,[13] analogous to UO_{2+x}, and has also caused some difficulty in identifying the correct behavior.[14] Herein we report on local structure and valence in the $PuO_{2+x−y}(OH)_{2y}\cdot z(H_2O)$ system, with PuO_2 samples prepared by a variety of methods, in more complete form than our earlier report.[15]

The PuO_{2+x} problem originates in the more general one whereby the uniquely high polarizability of oxygen in combination with the ability of transition metals to sustain multiple valences and geometries complicates the structural chemistry of metal oxides.[16] Cooperative effects, i.e., ordering of charge and the associated structural inhomogeneities including adventitious O atoms,[17,18] can result in phase separation and nanoscale heterogeneity that may give only small or even negligible signatures in diffraction patterns.[19] These structural properties correlate with the compelling properties of many complex oxides[20] and other materials.[21] They also afflict environmental chemistry, where oxide solubilities can span large ranges because of the variable incorporation of H_2O and the formation of inhomogeneous, surface-nucleated precipitates.[22] The actinides are primary examples of these phenomena. Hyper- and hypostoichiometric oxides are well known, even for many of the simple binary oxides. Although the *Fm3m* fluorite-structured AnO_2's are putatively the most stable material under normal conditions in equilibrium with H_2O, U, Np, and Pu actually exhibit continuous An:O ratios. U goes all the way to UO_3, with intermediate U_4O_9, U_3O_7, and U_3O_8 identified as separate crystallographic phases.[23] The highest Np oxide is Np_2O_5, whereas now that valences greater than IV have been demonstrated for Pu, it appears to stop at Pu_4O_9 with only a slight lattice expansion.[3] Scattering studies on UO_{2+x} for $x < 0.5$ culminated in the proposed Willis distortion.[24,25] The extra O atoms cluster as chains so that they remain at relatively long (>2.2 Å) distances from the nondisplaced U atoms. This simple structural model has subsequently evolved into a more extended one in which the adventitious O atoms join with the original ones to form cuboctahedral groups that organize into larger clusters.[26] This structure retains many of the chemical aspects of the original: the use of the octahedral holes as locations for the extra O atoms, the conservation of the U sublattice, and the absence of U−O bonds <2.19 Å. The clustering attribute of these models provides a smooth transition to U_4O_9 (and U_3O_7) because these clusters coalesce into the homogeneous higher valence oxide. Another vital aspect of these models is that the increased charge is accommodated by relatively small reduction in U−O distances while maintaining high coordination numbers (8 in the middle and 9 at the ends of the chains) of multiply bridging O atoms, whereas the precedents in coordination chemistry and actinates involve substantial bond contractions, often with the formation of "oxo" groups (multiply bound O anions with short U−O distances <1.8 Å that, in most molecular complexes, are inert and nonbridging and occur in pairs as trans-dioxo complexes with O−An−O angles near 180°), and reduced coordination numbers.

The significance of these scattering studies is that crystallography is sensitive to periodic aspects of structures, giving the long-range average positions of the atoms in the unit cells and not their individual positions with respect to each other.[18,19] Local structure measurements may therefore, in principle, provide a more accurate description of the structure when it contains a complicated, aperiodic, multisite distribution of the O atoms,[27] especially in terms of information associated with chemical speciation and valence. This has now been demonstrated for the PuO_{2+x} system, where XAFS measurements[15] have shown that the excess O is incorporated as Pu(V) oxo groups (the same configuration as for U, except that the bond lengths with stable Pu(V) are typically 0.10 Å longer than for Pu(VI)). These differences are significant not only scientifically but also because of the use of PuO_2 as fuel in nuclear reactors,

(5) Runde, W.; Conradson, S. D.; Efurd, D. W.; Lu, N. P.; Van Pelt, C. E. Tait, C. D. *Appl. Geochem.* **2002**, *17*, 837.

(6) Madic, C. *Science* **2000**, *287*, 243.

(7) Haschke, J. M.; Ricketts, T. E. *J. Alloys Compd.* **1997**, *252*, 148. Haschke, J. M.; Martz, J. C. *J. Alloys Compd.* **1998**, *266*, 81. Haschke, J. M.; Allen, T. H.; Martz, J. C. *J. Alloys Compd.* **1998**, *271*, 211.

(8) Haschke, J. M.; Allen, T. H.; Morales, L. A. *J. Alloys Compd.* **2001**, *314*, 78.

(9) Haschke, J. M.; Allen, T. H. *J. Alloys Compd.* **2002**, *36*, 124.

(10) Haschke, J. M.; Oversby, V. M. *J. Nucl. Mater.* **2002**, *305*, 187.

(11) Conradson, S. D. *Appl. Spectrosc.* **1998**, *52*, A252.

(12) Paffett, M. T.; Farr, D.; Kelly, D. *AIP Conf. Proc.* **2003**, *673*, 193.

(13) Petit, L.; Svane, A.; Szotek, Z.; Temmerman, W. M. *Science* **2003**, *301*, 498.

(14) Martin, P.; Grandjean, S.; Ripert, M.; Freyss, M.; Blanc, P.; Petit, T. *J. Nucl. Mater.* **2003**, *320*, 138.

(15) Conradson, S. D.; Begg, B. D.; Clark, D. L.; Den Auwer, C.; Espinosa-Faller, F. J.; Gordon, P. L.; Hess, N. J.; Hess, R.; Keogh, D. W.; Morales, L. A.; Neu, M. P.; Runde, W.; Tait, C. D.; Veirs, D. K.; Villella, P. M. *Inorg. Chem.* **2003**, *42*, 3715.

(16) Bussmann-Holder, A.; Simon, A.; Buttner, H.; Bishop, A. R. *J. Supercon.* **2000**, *13*, 491.

(17) Cao, W.; Krumhansl, J. A.; Gooding, R. J. *Phys. Rev. B: Condens. Matter* **1990**, *41*, 4334. Bishop, A. R.; Lookman, T.; Saxena, A.; Shenoy, S. R. *Europhys. Lett.* **2003**, *63*, 289.

(18) Lookman, T.; Saxena, A.; Dimitrov, D. A.; Bishop, A. R.; Albers, R. C. *Phys. Rev. B: Condens. Matter* **2000**, *62*, 5265.

(19) Garcia-Adeva, A. J.; Conradson, D. R.; Villella, P.; Conradson, S. D. *J. Phys. Chem. B* **2003**, *107*, 6704.

(20) Tranquada, J. M.; Sternlieb, B. J.; Axe, J. D.; Nakamura, Y.; Uchida, S. *Nature* **1995**, *375*, 561. Bianconi, A.; Saini, N. L.; Rosseti, T.; Lanzara, A.; Perali, A.; Missori, M.; Oyanagi, H.; Yamaguchi, H.; Nishihara, Y.; Ha, D. H. *Phys. Rev. B: Condens. Matter* **1996**, *54*, 12018. Egami, T.; Louca, D. *Phys. Rev. B: Condens. Matter* **2002**, *65*, 94422.

(21) Tyson, T. A.; Conradson, S. D.; Farrow, R. F. C.; Jones, B. A. *Phys. Rev. B: Condens. Matter* **1996**, *54*, R3702. Szunyogh, L.; Weinberger, P.; Sommers, C. *Phys. Rev. B: Condens. Matter* **1999**, *60*, 11910.

(22) Towle, S. N.; Bargar, J. R.; Brown, G. E.; Parks, G. A. *J. Colloid Interface Sci.* **1997**, *187*, 62.

(23) Allen, G. C.; Tempest, P. A. *Proc. R. Soc. London, A* **1986**, *406*, 325.

(24) Willis, B. T. M. *J. Chem. Soc., Faraday Trans.* **1987**, *83*, 1079.

(25) Murray, A. D.; Willis, B. T. M. *J. Solid State Chem.* **1990**, *84*, 52.

(26) Bevan, D. J. M.; Greis, O.; Strahle, J. *Acta Crystallogr., Sect. A* **1980**, *36*, 889. Bevan, D. J. M.; Grey, I. E.; Willis, B. T. M. *J. Solid State Chem.* **1986**, *61*, 1. Nowicki, L.; Garrido, F.; Turos, A.; Thome, L. *J. Phys. Chem. Solids* **2000**, *61*, 1789.

(27) Egami, T.; Billinge, S. J. L. *Prog. Mater. Sci.* **1994**, *38*, 359.

in power generators (Pu-238) for solar system and deep space exploration,[28] and as a long-term storage material.[29] Safe storage considerations have produced intense recent interest in surface and corrosion reactions of plutonium dioxide.[2] While plutonium is capable of forming coordination complexes with O ligands in its V, VI, and VII valences, it had been accepted that PuO$_2$ represented the highest obtainable binary oxide. The recent reports on higher-valent oxides such as PuO$_{2+x}$ in the solid state,[3,8] and PuO$_3$ [30] and PuO$_4$ [31] in the gas phase, demonstrate that the established views on the oxidation behavior of plutonium are worth reconsideration, and merit additional detailed study.[6]

Materials and Methods

Sample Preparation. The preparations of homogeneous, chemically ordered PuO$_2$ (called "cd") and PuO$_2$ solids by hydrolysis (referred to as "nitrate," "nitrate + NaCl", "nitrate + citrate", "aged", and "aged hydrothermal" colloids on the basis of their synthesis) and heterogeneous reduction from aqueous solution have been described.[15,32] Monoclinic CaZr$_{0.9}$Pu$_{0.1}$Ti$_2$O$_7$ and cubic CaZr$_{0.4}$Pu$_{0.6}$Ti$_2$O$_7$ were prepared by standard methods.[33] The preparations of PuO$_{2+x}$, including two samples of high-fired material (a and b), the formation of PuO$_{2.17}$, PuO$_{2.21}$, and PuO$_{2.26}$ from high-fired (a), the reaction of high-fired (b) that had been prepared by direct air oxidation of the metal with air at 15, 37, and 80% relative humidity to give the 15rh, 37rh, and 80rh samples, and the sample of low-fired material have been described.[15,32] PuO$_{2+x}$ from corroded metal was prepared by the room-temperature oxidation of 0.5 wt % Ga-stabilized δ Pu via exposure to H$_2$O vapor which contained approximately 0.05 Torr of HCl as a catalyst. This was maintained by exposing the metal to the vapor over an aqueous HCl solution overnight. The black oxide that was formed spalled from the metal and was collected for analysis. XRD showed that the material was crystalline, but the widths of the peaks indicated that the lattice was not well ordered. A sample of PuO$_{2.03}$ was prepared by the same reaction with H$_2$O vapor at 300 °C, but from substoichiometric starting material. The H$_2$ vs time plot showed a plateau (believed to be PuO$_{2.00}$); this sample was taken immediately after the evolution of H$_2$ resumed and so is believed to have $0.00 < x < 0.06$.

Acquisition and Analysis of XAFS Spectra. The data acquisition and preliminary analysis methods have been described.[32] The extended X-ray absorption fine structure (EXAFS) was extracted from the spectra by using a polynomial spline function to approximate the smooth atomic absorption. This was optimized by minimizing the area of the Fourier transform modulus from 0 to 1.1 Å. Substantial effort was made to use very similar polynomial spline parameters and obtain the same function for all spectra to minimize the effects of background artifacts on the curve-fitting results. Metrical results in terms of N, the numbers of atoms, r, the Pu$-$O(Pu) distances, and σ, the pairwise Debye$-$Waller factors, were obtained by curve-fits of the $\chi(k)$ data over the ranges depicted in the figures, which generally used the full spectral range available but are not identical for all samples. Fourier transforms ($\chi(R)$)

were performed over the same range, also using k^3 weighting to enhance the accuracy for the O shells, and a sine window. The number of independent parameters for the $k = 3.2-14.6$ Å^{-1} and $R = 1.2-4.6$ fitting ranges for these experiments is 27.[34] If the curve-fitting parameters are unconstrained, then this is only 2.7$-$3.4 degrees of freedom for each of the 8$-$10 crystallographic shells of atoms. After much trial and error, sets of constraints for ΔE_0's, σ's, and total numbers of atoms were found that were applied to all spectra from a particular class of compounds and significantly lowered the number of degrees of freedom in the fits. The ionization thresholds were set at 18062.0, 18063.0, or 18064.0 eV, whichever was closest to the inflection point of the edge. Pairwise Pu$-$O and Pu$-$Pu curve-fitting parameters were obtained using FEFF7.[35] The total spectrum was also calculated this way and then scaled to give the best match to the experimental spectra. The number of shells used is the same as in the table and does vary among the samples. Fits were typically begun with nine shells; the number was reduced if two shells either converged or destructively interfered with each other, and a tenth shell was added if a distinct feature still remained in the fit. Most spectra displayed a feature, which can be seen in the figures, that could be fit by an O shell near 3.6 Å, resulting in substantial overlap with the Pu shell. Because of this problem, and insofar as a shell at this distance has no effect on the conclusions drawn from this study, it was therefore neglected in all but a few spectra. For all spectra, ΔE_0 was fixed at 0.6 eV for all O shells with Pu$-$O <3.6 Å, fixed at 2.3 eV for the Pu shell, and allowed to float for the O shell at 4.47 Å. The Debye$-$Waller factors for the two or three largest O shells, which were typically the ones that composed the primary O shell with 2.15 < Pu$-$O < 2.45 Å, were allowed to float between 0.05 and 0.09 Å, although the range was smaller for some spectra. The Debye$-$Waller factors for all other O shells were set at the average value of these three or at 0.045$-$0.050 Å if a small value resulted in a significantly better fit. The total number of O atoms with Pu$-$O <3.6 Å was allowed to vary between 6.5 and 9.5, with this sum almost always reaching the 9.5 atom limit and the Debye$-$Waller factors tending toward their lower limits during the optimization, maximizing the amplitude of the individual waves at high k. The Debye$-$Waller factors for the Pu and 4.47 Å O shells were allowed to float, except that if the resulting number of atoms was too large or small they were fixed at values that gave a number consistent with others in the particular set of compounds.

Reported errors in the curve fit results (Table 1) for N, r, and σ (even when these did not float or were otherwise constrained in the fit) were derived by calculating the difference in the least-squares errors between a fit that included the wave in question and one that did not to get the contribution of that wave to the fit and then varying each parameter for that wave until the least-squares error was higher than the optimum by 10% of this contribution. This provides a fair representation of the sensitivity of the fit to an individual parameter. However, insofar as a major source of error in this analysis is correlation among the parameters from not only two but also three and more waves, the actual uncertainties for some parameters may be significantly larger. As is usual in EXAFS, the distances and other information originating in the phase will be more accurate than numbers, σ's, and amplitude-dependent results. Judicious selection of constraints prevented the total numbers of atoms from becoming unphysically large when the waves from nearby shells interfered with each other.

Results

PuO$_2$. The 5.396 Å lattice constant of PuO$_2$ gives a Pu partial pair distribution function (pdf, $g(r)$) of 8 nearest-neighbor O atoms at 2.336 Å, 12 Pu atoms at 3.816 Å, 24 O atoms at 4.474 Å, etc. This highly ordered structure results in a relatively simple $\chi(R)$ EXAFS spectrum through high R (Figure 1, note that R

(28) Angelo, J. A., Jr.; Buden, D. *Space Nuclear Power*; Orbit Book Co.: Malabar, FL, 1985. Rinehart, G. H. *Space Nucl. Power Syst.* **1992**, *10*, 39. Rinehart, G. H. *Prog. Nucl. Energy* **2001**, *39*, 305.
(29) Paffett, M. T.; Kelly, D.; Joyce, S. A.; Morris, J.; Veirs, D. K. *J. Nucl. Mater.* **2003**, *322*, 45.
(30) Ronchi, C.; Capone, F.; Colle, J. Y.; Hiernaut, J. P. *J. Nucl. Mater.* **2000**, *280*, 111. Krikorian, O. H.; Fontes, A. S., Jr.; Ebbinghaus, B. B.; Adamson, M. G. *J. Nucl. Mater.* **1997**, *247*, 161.
(31) Domanov, V. P.; Buklanov, G. V.; Lobanov, Y. V. *Radiokhimiya (Engl. Ed.)* **2002**, *44*, 114.
(32) Conradson, S. D.; Abney, K. D.; Begg, B. D.; Brady, E. D.; Clark, D. L.; Den Auwer, C.; Ding, M.; Dorhout, P. K.; Espinosa-Faller, F. J.; Gordon, P. L.; Hess, N. J.; Hess, R. F.; Keogh, D. W.; Lander, G. H.; Lupinetti, A. J.; Neu, M. P.; Palmer, P. D.; Paviet-Hartmann, P.; Reilly, S. D.; Runde, W. H.; Tait, C. D.; Veirs, D. K.; Wastin, F. *Inorg. Chem.* **2004**, *43*, 116.
(33) Begg, B. D.; Vance, E. R.; Conradson, S. D. *J. Alloys Compd.* **1998**, *271*, 221. Begg, B. D.; Vance, E. R.; Day, R. A.; Hambley, M.; Conradson, S. D. In *Scientific Basis for Nuclear Waste Management XX*; Gray, W. J., Triay, I. R., Eds.; Materials Research Society: Warrendale, PA, 1997; p 325.
(34) Stern, E. A. *Phys. Rev. B: Condens. Matter* **1993**, *48*, 9825.
(35) Ankudinov, A. L.; Rehr, J. J. *Phys. Rev. B: Condens. Matter* **1997**, *56*, R1712.

Table 1. Metrical Parameters from Curve Fits with 2–9 O and 1 Pu Shells[a]

sample	param	O shells Pu–O <3.6 Å								Pu	O at 4.5 Å
Crystal Structure		2.3368								3.81612	4.47424
Ordered PuO₂ by Chemical Decomposition											
PuO₂ - cd sample 1	R	2.34 ± 0.02								3.83 ± 0.01	4.53 ± 0.02
	N	7.4 ± 2.1								10.0 ± 2.4	23.0 ± 7.2
	σ	0.076 ± 0.013								0.067 ± 0.007	0.087 ± 0.012
PuO₂ - cd sample 2	R	2.33 ± 0.02								3.82 ± 0.01	4.53 ± 0.02
	N	7.2 ± 2.1								8.9 ± 2.2	14.9 ± 4.7
	σ	0.077 ± 0.013								0.056 ± 0.007	0.077 ± 0.012
Heat-Treated Compounds											
high-fired (a)	R	1.96 ± 0.02	2.26 ± 0.02	2.76 ± 0.02	2.98 ± 0.02	3.27 ± 0.02				3.82 ± 0.01	4.41 ± 0.02
	N	0.1 ± 0.0	3.0 ± 0.9	1.7 ± 0.6	1.4 ± 0.6	0.4 ± 0.1				9.0 ± 2.3	16.4 ± 5.1
	σ	0.050 ± 0.008	0.050 ± 0.014	0.050 ± 0.016	0.050 ± 0.009	0.050 ± 0.006				0.062 ± 0.007	0.080 ± 0.012
x = 0.03	R	1.91 ± 0.02	2.29 ± 0.02	2.81 ± 0.02	3.02 ± 0.02	3.33 ± 0.02				3.82 ± 0.01	4.49 ± 0.02
	N	0.3 ± 0.1	4.2 ± 1.2	2.0 ± 0.6	0.9 ± 0.3	0.7 ± 0.3				7.4 ± 1.9	9.2 ± 2.9
	σ	0.050 ± 0.014	0.077 ± 0.012	0.076 ± 0.015	0.076 ± 0.017	0.076 ± 0.006				0.077 ± 0.006	0.086 ± 0.012
x = 0.17	R	1.91 ± 0.01	2.35 ± 0.02	2.71 ± 0.02	2.94 ± 0.016	3.31 ± 0.02	3.54 ± 0.01			3.84 ± 0.01	4.56 ± 0.02
	N	0.3 ± 0.1	5.3 ± 1.5	0.6 ± 0.2	0.3 ± 0.1	0.8 ± 0.3	1.0 ± 0.3			7.9 ± 2.0	17.0 ± 5.3
	σ	0.050 ± 0.015	0.071 ± 0.013	0.051 ± 0.013	0.051 ± 0.010	0.051 ± 0.014	0.051 ± 0.015			0.061 ± 0.006	0.088 ± 0.013
x = 0.21	R	1.85 ± 0.02	2.37 ± 0.02	2.74 ± 0.02	2.99 ± 0.02	3.30 ± 0.02				3.82 ± 0.01	4.51 ± 0.02
	N	0.5 ± 0.2	3.4 ± 1.0	0.7 ± 0.2	0.5 ± 0.2	1.0 ± 0.4				7.4 ± 1.8	14.7 ± 4.6
	σ	0.050 ± 0.015	0.073 ± 0.013	0.053 ± 0.014	0.053 ± 0.014	0.053 ± 0.008				0.070 ± 0.006	0.090 ± 0.011
x = 0.26	R	1.84 ± 0.2	2.13 ± 0.02	2.28 ± 0.01	2.41 ± 0.01	2.73 ± 0.02	2.94 ± 0.02	3.19 ± 0.02	3.37 ± 0.02	3.83 ± 0.01	4.38 ± 0.02
	N	0.5 ± 0.2	1.0 ± 0.3	3.1 ± 0.9	1.8 ± 0.6	0.4 ± 0.2	1.1 ± 0.3	1.2 ± 0.4	0.4 ± 0.2	10.4 ± 2.6	23.2 ± 7.5
	σ	0.050 ± 0.014	0.050 ± 0.014	0.055 ± 0.012	0.055 ± 0.014	0.053 ± 0.015	0.053 ± 0.015	0.050 ± 0.015	0.050 ± 0.015	0.080 ± 0.007	0.080 ± 0.011
corroded metal	R	1.93 ± 0.02	2.21 ± 0.03	2.74 ± 0.02	2.97 ± 0.02	3.27 ± 0.02				3.81 ± 0.02	4.61 ± 0.03
	N	0.4 ± 0.1	2.6 ± 0.8	1.3 ± 0.4	1.9 ± 0.6	1.6 ± 0.5				7.7 ± 2.3	9.8 ± 3.1
	σ	0.050 ± 0.015	0.090 ± 0.015	0.080 ± 0.014	0.080 ± 0.015	0.080 ± 0.007				0.080 ± 0.007	0.080 ± 0.011
low-fired	R	1.78 ± 0.01	2.27 ± 0.02	2.39 ± 0.02	2.68 ± 0.002	2.86 ± 0.02	3.07 ± 0.02	3.31 ± 0.02		3.84 ± 0.01	4.59 ± 0.02
	N	<0.1	2.8 ± 0.9	2.3 ± 0.8	1.4 ± 0.4	1.6 ± 0.4	0.9 ± 0.2	0.4 ± 0.1		7.1 ± 1.8	15.8 ± 5.3
	σ	0.050 ± 0.007	0.050 ± 0.014	0.050 ± 0.014	0.050 ± 0.011	0.055 ± 0.006	0.080 ± 0.015	0.080 ± 0.015		0.059 ± 0.006	0.100 ± 0.013
high-fired (b)	R	1.88 ± 0.01	2.28 ± 0.02	2.78 ± 0.03	3.34 ± 0.01					3.83 ± 0.01	4.49 ± 0.02
	N	0.3 ± 0.1	4.0 ± 1.2	1.9 ± 0.6	1.0 ± 0.3					7.2 ± 1.7	17.9 ± 5.6
	σ	0.050 ± 0.015	0.081 ± 0.014	0.050 ± 0.013	0.067 ± 0.005					0.062 ± 0.006	0.101 ± 0.012
15% humidity	R	1.85 ± 0.02	2.14 ± 0.02	2.32 ± 0.02	2.81 ± 0.02	3.34 ± 0.02				3.83 ± 0.01	4.50 ± 0.02
	N	0.5 ± 0.2	1.6 ± 0.6	6.7 ± 2.0	1.9 ± 0.6	0.5 ± 0.1				8.2 ± 2.0	18.5 ± 5.8
	σ	0.050 ± 0.015	0.081 ± 0.014	0.050 ± 0.013	0.067 ± 0.011	0.067 ± 0.005				0.063 ± 0.006	0.086 ± 0.011
37% humidity	R	1.89 ± 0.02	2.13 ± 0.02	2.26 ± 0.01	2.72	2.87	3.08 ± 0.02	3.32 ± 0.02		3.83 ± 0.01	4.51 ± 0.02
	N	0.6 ± 0.2	0.7 ± 0.1	3.0 ± 0.8	0.2	0.5	0.4 ± 0.1	0.9 ± 0.2		9.2 ± 2.2	19.1 ± 6.0
	σ	0.050 ± 0.007	0.050 ± 0.007	0.045 ± 0.014	0.045	0.045	0.050 ± 0.003	0.050 ± 0.005		0.064 ± 0.006	0.085 ± 0.011
80% humidity	R	1.88 ± 0.01	2.19 ± 0.02	2.33 ± 0.02	2.77 ± 0.02	3.33 ± 0.02				3.83 ± 0.01	4.49 ± 0.02
	N	0.7 ± 0.2	2.1 ± 0.3	5.8 ± 1.7	0.2 ± 0.1	0.7 ± 0.3				8.8 ± 2.1	22.8 ± 6.9
	σ	0.050 ± 0.014	0.090 ± 0.014	0.073 ± 0.012	0.059 ± 0.013	0.050 ± 0.005				0.063 ± 0.006	0.094 ± 0.012
Aqueous Precipitates: Hydrolysis											
nitrate + NaCl	R	1.86 ± 0.01	2.21 ± 0.01	2.36 ± 0.02	2.84 ± 0.02	3.04 ± 0.02	3.28 ± 0.02			3.82 ± 0.01	4.41 ± 0.02
	N	0.6 ± 0.2	2.0 ± 0.5	3.9 ± 0.9	0.6 ± 0.2	1.3 ± 0.4	1.1 ± 0.4			6.6 ± 1.7	5.2 ± 1.6
	σ	0.050 ± 0.010	0.052 ± 0.013	0.073 ± 0.011	0.053 ± 0.010	0.053 ± 0.017	0.053 ± 0.018			0.087 ± 0.008	0.080 ± 0.012

Table 1. (Continued)

In the table below, each sample lists, top-to-bottom within a cell, the interatomic distance R (Å), coordination number N, and Debye–Waller factor σ² (Å²), each with its uncertainty. The six O-shell columns fall under the heading "O shells Pu–O <3.6 Å."

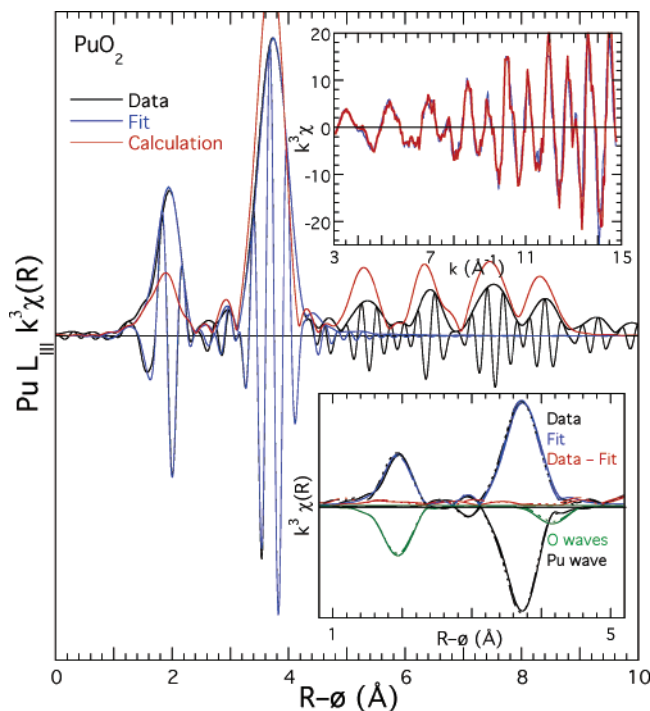| sample	O shell	O shell	O shell	O shell	O shell	O shell	Pu	O at 4.5 Å
nitrate	1.83 ± 0.02	2.22 ± 0.01	2.38 ± 0.02	2.84 ± 0.02	3.05 ± 0.02	3.29 ± 0.02	3.82 ± 0.02	4.47 ± 0.02
	0.4 ± 0.1	2.4 ± 0.6	3.8 ± 1.0	0.4 ± 0.2	1.2 ± 0.4	1.3 ± 0.4	7.8 ± 2.1	5.4 ± 1.7
	0.050 ± 0.009	0.054 ± 0.013	0.068 ± 0.011	0.055 ± 0.010	0.055 ± 0.016	0.044 ± 0.019	0.089 ± 0.008	0.080 ± 0.012
nitrate + citrate	1.83 ± 0.02	2.23 ± 0.01	2.39 ± 0.02	2.82 ± 0.02	3.06 ± 0.2	3.31 ± 0.02	3.82 ± 0.02	4.40 ± 0.02
	0.6 ± 0.2	3.1 ± 0.8	3.4 ± 0.9	0.9 ± 0.2	0.8 ± 0.1	0.7 ± 0.1	4.2 ± 1.2	10.0 ± 3.1
	0.050 ± 0.007	0.050 ± 0.014	0.050 ± 0.014	0.050 ± 0.007	0.050 ± 0.006	0.050 ± 0.006	0.079 ± 0.010	0.100 ± 0.014
aged	1.88 ± 0.01	2.19 ± 0.02	2.35 ± 0.02	2.77 ± 0.02	3.04 ± 0.04	3.31 ± 0.02	3.82 ± 0.01	4.56 ± 0.015
	0.4 ± 0.1	2.0 ± 0.4	5.0 ± 1.9	0.3 ± 0.1	0.6 ± 0.1	1.2 ± 0.4	5.8 ± 1.6	4.4 ± 1.5
	0.050 ± 0.005	0.070 ± 0.013	0.087 ± 0.014	0.053 ± 0.08	0.098 ± 0.023	0.053 ± 0.014	0.069 ± 0.008	0.080 ± 0.003
aged hydrothermal	1.82 ± 0.02	2.19 ± 0.02	2.36 ± 0.02	2.78 ± 0.02	3.03 ± 0.02	3.32 ± 0.02	3.82 ± 0.01	4.53 ± 0.02
	0.4 ± 0.1	1.5 ± 0.5	4.4 ± 1.3	0.9 ± 0.4	1.0 ± 0.2	1.1 ± 0.2	6.7 ± 1.7	8.7 ± 2.7
	0.050 ± 0.006	0.050 ± 0.015	0.069 ± 0.013	0.054 ± 0.007	0.054 ± 0.008	0.054 ± 0.008	0.055 ± 0.009	0.080 ± 0.012
Aqueous Precipitates: Reduction								
5 M NaCl + Fe	1.84 ± 0.02	2.25 ± 0.02	2.38 ± 0.02	2.80 ± 0.02	3.01 ± 0.02	3.33 ± 0.02	3.80 ± 0.01	4.40 ± 0.02
	0.4 ± 0.1	4.9 ± 1.1	3.6 ± 1.0	0.7 ± 0.3	0.4 ± 0.1	0.5 ± 0.1	7.0 ± 1.9	8.2 ± 2.6
	0.050 ± 0.010	0.074 ± 0.013	0.073 ± 0.013	0.055 ± 0.011	0.055 ± 0.010	0.055 ± 0.005	0.079 ± 0.010	0.080 ± 0.012
5 M NaCl + Fe + NaOCl	0	2.25 ± 0.02	2.37 ± 0.02	2.78 ± 0.02	3.04 ± 0.02	3.32 ± 0.02	3.81 ± 0.01	4.36 ± 0.02
		3.7 ± 1.2	3.9 ± 1.3	0.6 ± 0.1	0.4 ± 0.1	0.8 ± 0.2	7.0 ± 2.0	9.2 ± 2.9
		0.088 ± 0.015	0.088 ± 0.015	0.055 ± 0.006	0.055 ± 0.005	0.055 ± 0.025	0.075 ± 0.009	0.080 ± 0.011
ERDA + Fe	1.87 ± 0.02	2.25 ± 0.02	2.37 ± 0.02	2.79 ± 0.02	2.98	3.35 ± 0.02	3.79 ± 0.01	4.42 ± 0.02
	0.7 ± 0.2	3.3 ± 0.9	3.5 ± 1.1	0.5 ± 0.2	0.5	0.9 ± 0.4	2.8 ± 0.09	4.7 ± 1.5
	0.050 ± 0.012	0.064 ± 0.013	0.065 ± 0.013	0.055 ± 0.008	0.055	0.055 ± 0.018	0.054 ± 0.011	0.080 ± 0.013
ERDA + Fe + NaOCl	1.81 ± 0.01	2.24 ± 0.02	2.37 ± 0.02	2.76 ± 0.02	2.98 ± 0.02	3.36 ± 0.02	3.80 ± 0.01	4.62 ± 0.02
	0.1 ± 0.0	3.9 ± 1.1	4.1 ± 1.2	0.5 ± 0.2	0.3 ± 0.2	1.2 ± 0.4	2.1 ± 0.6	3.5 ± 1.1
	0.050 ± 0.004	0.090 ± 0.015	0.091 ± 0.015	0.050 ± 0.008	0.055 ± 0.007	0.055 ± 0.018	0.063 ± 0.011	0.080 ± 0.014
ERDA + Al	1.82 ± 0.12	2.23 ± 0.02	2.38 ± 0.02	2.84 ± 0.02	3.02 ± 0.02	3.37 ± 0.02	3.81 ± 0.02	4.38 ± 0.02
	0.2 ± 0.1	3.8 ± 0.9	4.2 ± 1.0	0.6 ± 0.2	0.6 ± 0.2	0.1 ± 0.0	2.8 ± 0.8	5.4 ± 1.6
	0.050 ± 0.010	0.088 ± 0.011	0.086 ± 0.011	0.055 ± 0.015	0.055 ± 0.018	0.055 ± 0.004	0.080 ± 0.014	0.080 ± 0.013
ERDA + Al + NaOCl	1.77 ± 0.02	2.16 ± 0.02	2.30 ± 0.01	2.86 ± 0.02	3.06 ± 0.02	3.32 ± 0.02	3.79 ± 0.02	4.37 ± 0.02
	0.2 ± 0.1	1.4 ± 0.4	4.5 ± 1.0	0.6 ± 0.3	0.8 ± 0.3	0.4 ± 0.1	5.9 ± 1.6	6.0 ± 1.9
	0.050 ± 0.016	0.074 ± 0.012	0.074 ± 0.010	0.065 ± 0.016	0.055 ± 0.016	0.055 ± 0.006	0.108 ± 0.011	0.080 ± 0.012
Substitutional Compounds								
CaZr$_{0.9}$Pu$_{0.1}$Ti$_2$O$_7$	1.89 ± 0.02	2.18 ± 0.02	2.36 ± 0.02	2.44 ± 0.01	2.79 ± 0.02	3.06 ± 0.02		
	0.5 ± 0.2	3.1 ± 0.9	2.5 ± 0.8	1.6 ± 0.4	1.2 ± 0.5	0.6 ± 0.3		
	0.050 ± 0.015	0.072 ± 0.013	0.083 ± 0.015	0.055 ± 0.013	0.083 ± 0.015	0.070 ± 0.016		
CaZr$_{0.4}$Pu$_{0.6}$Ti$_2$O$_7$	1.88 ± 0.02	2.14 ± 0.02	2.27 ± 0.01	2.42 ± 0.02	2.82 ± 0.02	3.06 ± 0.02		
	0.4 ± 0.1	2.5 ± 0.8	0.7 ± 0.2	4.3 ± 1.3	0.6 ± 0.2	0.6 ± 0.3		
	0.050 ± 0.014	0.095 ± 0.015	0.045 ± 0.014	0.088 ± 0.015	0.067 ± 0.014	0.070 ± 0.016		

Figure 1. $k^3\chi(R)$ EXAFS (modulus and real component) of two samples of PuO_2 prepared via decomposition of KPu_2Se_6 and the modulus calculated from the crystal structure. The peak positions are phase-shifted to lower distance from the actual Pu−O/Pu distances, with the Pu−O shifted by more than the Pu−Pu. The calculated spectrum has been reduced in size to more closely match the experimental ones, which have much larger Debye−Waller factors for the Pu and more distant shells. The insets show the two $k^3\chi(k)$ spectra (blue and red) and the two $k^3\chi(R)$ moduli (solid and dash−dot) overlaid with curve-fits that include the first three O, Pu, and O shells through 4.4 Å. These individual components of the fit have been inverted for clarity.

refers to the abcissa in a plot of χ and therefore the position of features in the Fourier transform representation of the EXAFS, whereas r refers to actual distances between atom pairs). The two individual PuO_2 samples made by decomposition of KPu_2-Se_6 by the extended high-temperature oxidation with the SiO_2 and residual O in the container under rigorously anhydrous conditions exhibit virtually identical spectral features (and, by implication, structures) through $R = 6$ Å, and remain quite similar even at higher distances. The high degree of ordering is reflected in the large, reproducible contributions from the more distant shells, which lose amplitude very quickly (vide infra) as atoms become displaced from the lattice. It is also signified by the excellent correspondence with the calculation from the fully ordered structure even through $R = 8$ Å and beyond. The amplitude of the nearest-neighbor O contribution relative to that for the Pu (and the more distant shells) in the experimental spectra is much larger than in the calculated spectrum because its combined thermal plus static Debye−Waller factor is lower than those for the more distant shells, whereas the calculation uses the same Debye−Waller factor for every pair. This effect is exaggerated by the k^3 weighting, which also greatly magnifies the sensitivity of the Pu amplitude in the transform to the Pu−Pu Debye−Waller factor. The important aspect of the comparison with the calculation, ignoring the total amplitudes, is the fact that every feature in it, including the nodes of the real part (not shown), is matched in the experimental spectra. Differences between the structures of the samples and the homogeneous crystallographic one are thus minor to negligible.
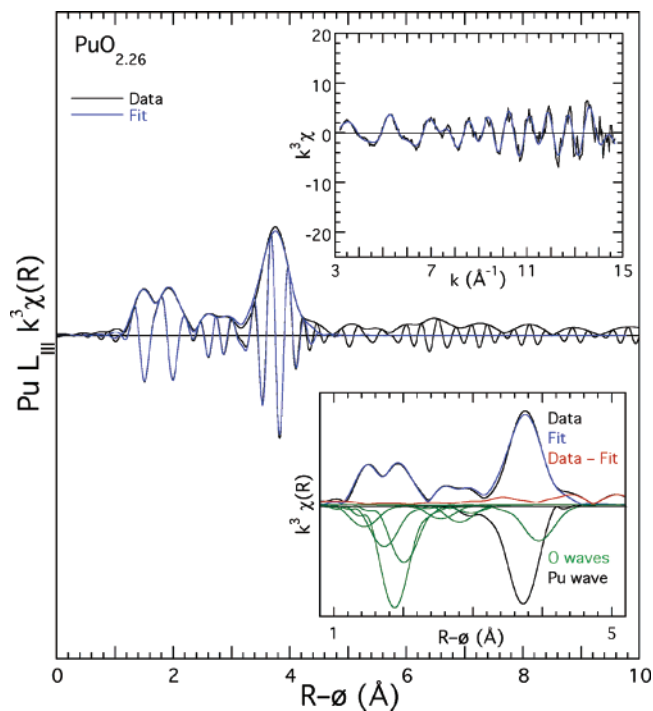
Figure 2. $k^3\chi(R)$ of the EXAFS of and 10-shell fit to the spectrum of $PuO_{2.26}$ prepared by reaction of high-fired (a) with H_2O vapor at elevated temperature. The modulus and real part of the transform of both the data and fit are shown. The insets show the $k^3\chi$ spectrum overlaid with the curve-fit and the moduli of the data, fit, difference between the data and fit, and the individual contributions to the fit (inverted for clarity). The vertical scales of the main and $k^3\chi$ plots are identical to those in Figure 1.

The close correspondence of the local and crystallographic structures is corroborated by the curve fits (Figure 1), which include the three crystallographic, O, Pu, and O shells through the O at 4.5 Å. Although the residual is not completely flat, there are no distinct features of significant amplitude that are not fit with the crystallographic model. Because the Debye−Waller factors for the three shells are independent, the curve-fit, unlike the calculation, matches the experimental amplitudes for each shell and tracks the real part much more closely from $R = 2.3$−2.6 Å, the region between the nearest-neighbor O and Pu shells. The low numbers of atoms found by the fits (Table 1) for the Pu and 4.5 Å O shell at least partly reflect, as displayed in the results, $N−\sigma$ correlation. Fixing the number of atoms at the larger crystallographic values results in larger σ's while also giving good fits because the minima are shallow along the $N−\sigma$ surface in the fitting space. This uniqueness problem follows not only from the relative uncertainty in the low k amplitude of the Pu−Pu wave, which determines N while the high k amplitude determines σ, but may also indicate some thermal and/or static anharmonicity in the Pu−Pu and Pu−$O_{4.5\ Å}$ distributions. This rationale, together with the extreme sensitivity of σ in the k^3-weighted fit, also accounts for the counterintuitive finding of a Debye−Waller factor for the O that is larger than that for the Pu.

$PuO_{2.26}$. The decoupling of long-range average and local structure is demonstrated by the fact that $PuO_{2.26}$ gives the same diffraction pattern as the other samples with only a slight increase in lattice constant. The local disorder and variation from the PuO_2 structure are apparent in the reduced amplitude of the $\chi(k)$ spectrum and amplitude reduction and the absence of high-R features in $\chi(R)$ (Figure 2). Below $R = 3.2$ Å, however, the

spectrum differs from that of ordered PuO$_2$ more fundamentally. The size of the low-R component of the primary O peak in the absence of any experimental errors that would produce a low frequency in the $\chi(R)$, its invariance with different spline polynomial parameters, and, vide infra, its excellent fit with a combination of Pu—O waves demonstrate that it does originate in an atom shell and not an error in the spectrum or background subtraction process. The $R = 2$ Å position of the upper peak is close to that of the O peak in the PuO$_2$ spectrum, and the pattern displayed by its real part is also similar. The lower peak, however, is near $R = 1.4$ Å. Furthermore, its real part, instead of exhibiting an asymmetric valley at $R = 1.6$ Å that begins with a low, broadened peak at $R = 1.4$ Å as for ordered PuO$_2$, begins with a high, narrow peak that descends into a symmetric valley near the same position or slightly lower. The complexity of the spectrum demonstrates that the nearest-neighbor O distribution in this compound is complicated and multisite, with ordered subshells occurring at distances both above and below that of the 2.3 Å PuO$_2$-like distance.

The Pu and O at 4.47 Å contributions are well fit by single shells near the crystallographic distances (Table 1). Although the magnitude of the combined Pu/O at 4.47 Å (modulus peak at $R = 3.75$ Å) feature in the $\chi(R)$ spectrum is almost uniquely low for the subset of compounds treated at high temperature, the curve-fit nevertheless finds large Debye—Waller factors and numbers of atoms that are therefore closer to the crystallographic values than for many other samples. Given the extended disorder in the compound, it is somewhat surprising that so many of the apparently full contingent of Pu atoms are found by the fit, spread over a broad but still harmonic distribution. This result gives credibility to the lower occupancies in these shells found for the precipitated compounds (vide infra) and the expectation that treatment at high temperature condenses the material on the atomic scale. Structural differences between this and the other high-temperature compounds must therefore reside in the nearest-neighbor O shells and the speciation of the directly coordinated O atoms.

Fitting the entire nearest-neighbor O contribution requires eight O shells of varying numbers of atoms from 1.8 to 3.4 Å. This high number implies that the complexity of the structure increases as the O excess limit is attained. Some shifts in the Pu—O distances (Figure 2) are also observed at this high value of x. Insofar as some pairs of shells overlap and others may be separated by distances close to the 0.15 Å value that results in maximum destructive interference between the waves, the g(r)/rdf graphical presentation of the curve-fit results is likely to be a more accurate depiction and a better basis for interpretation of the local structure than explicit use of the tabulated curve-fitting values.[36]

The two peaks of the nearest-neighbor O contribution that require four Pu—O waves to be completely fit, of which the one with the most atoms is actually almost twice as large in magnitude as the features in the spectrum, provide an example of the effects of overlap. The distribution around 2.3 Å is therefore actually described as very broad and asymmetric, tailing off more slowly and extending farther on its lower side. This indicates a wide range of Pu—O bond types involving different O species as well. The O shell at 1.84 Å is, however,
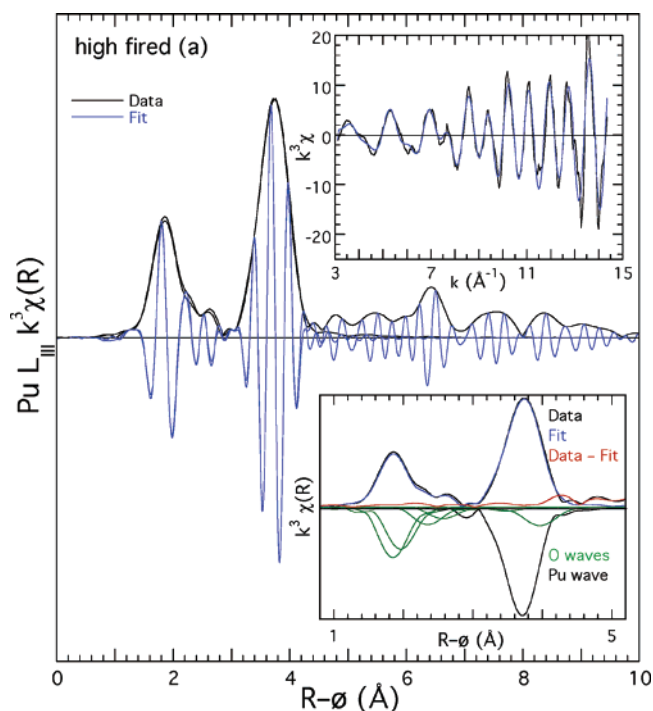
(36) Tyson, T. A.; deLeon, J. M.; Conradson, S. D.; Bishop, A. R.; Neumeier, J. J.; Roder, H.; Zang, J. *Phys. Rev. B: Condens. Matter* **1996**, *53*, 13985.
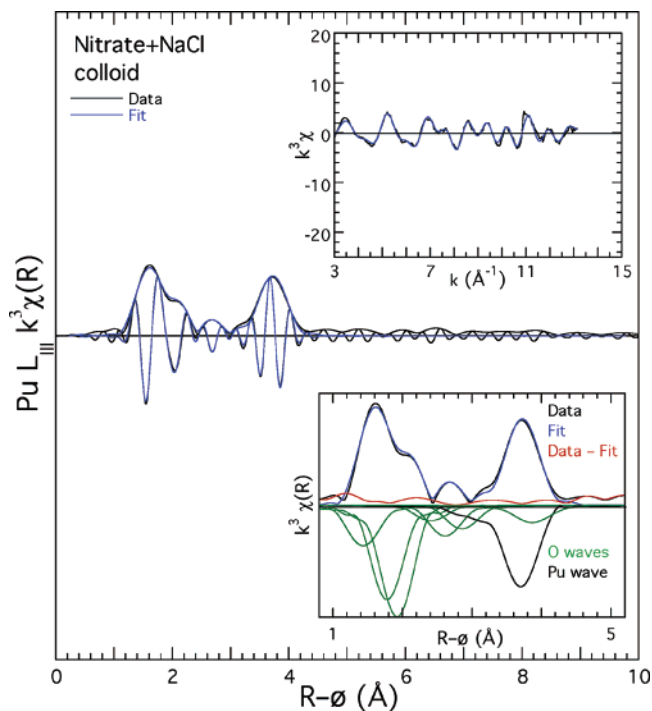

Figure 3. $k^3\chi(R)$ of the EXAFS of and eight-shell fit to PuO$_2$—high-fired (a). The modulus and real part of the transform of both the data and fit are shown. The insets show the $k^3\chi$ spectrum overlaid with the curve-fit and the moduli of the data, fit, difference between the data and fit, and the individual contributions to the fit (inverted for clarity). The vertical scales of the main and $k^3\chi$ plots are identical to those in Figures 1 and 2.

the characteristic in the distribution of most interest because of its implications for the excess O. It is completely separated from the other O atoms and is therefore mostly independent from them in the spectrum. This is demonstrated by the lower R peak in the spectrum being only ca. 0.1 Å above that of the O at 1.84 Å, which can clearly be seen to give a positive contribution to the transform modulus that enhances the magnitude of the low-R peak in the data. Since the low-R peak is then primarily the spectral contribution of this shell, there is no alternative to an O at 1.84 Å in obtaining a complete fit to the data. The presence of this feature in the spectrum is therefore unambiguously the result of the O shell at <1.9 Å. This is critical because its sets a necessary precedent for identifying an identical shell in the spectra of other samples where this oxo shell does not give a clearly resolved low-R feature.

Additional Characteristics of Oxo Moieties. Two compounds in addition to that of ordered PuO$_2$ that do not show an O shell at 1.8—1.9 Å in their EXAFS are the high-fired (a) (Figure 3) and the precipitate reduced by solid Fe metal in 5 M NaCl solution with NaOCl. Both of these show a certain pattern in the lower R portion of the real parts of their $\chi(R)$ spectra, despite differences in the shapes of the modulus, that is not the same as that in the spectrum of PuO$_{2.26}$. The modulus peak positions from the primary O shell occur near $R = 1.8$ Å. The real part of the transform is very low and flat when it is positive around $R = 1.4$ Å before dipping into a deep, asymmetric valley around $R = 1.6$ Å. In contrast, the comparable modulus peak positions in, e.g., the nitrate + NaCl colloid (Figure 4) and, e.g., PuO$_{2.17}$ $\chi(R)$ spectra that do give oxo shells are, respectively, at $R = 1.9$ and 1.6 Å, with shoulders on the low- and high-R sides. Differing from the non-oxo spectra but similar to the spectrum of PuO$_{2.26}$, the real components have high peaks

Figure 4. $k^3\chi(R)$ of the EXAFS of and nine-shell fit to the spectrum of the nitrate + NaCl colloid prepared by hydrolysis. The modulus and real part of the transform of both the data and fit are shown. The insets show the $k^3\chi$ spectrum overlaid with the curve-fit and the moduli of the data, fit, difference between the data and fit, and the individual contributions to the fit (inverted for clarity). The vertical scales of the main and $k^3\chi$ plots are identical to those in Figures 1 and 2.

at $R = 1.4$ Å before descending into deep, symmetric valleys at $R = 1.6$ Å that render them distinctly similar to the $PuO_{2.26}$ spectrum. These two patterns therefore correlate strongly with, respectively, the absence and presence of the short Pu–O distance.

A necessary but not necessarily sufficient condition for the presence of the very short, highly controversial O shell is that the component of the spectrum being fit must not only improve the fit by its inclusion but also exhibit the Pu–O amplitude and phase. Subtracting the other waves of the fit from the spectrum isolates the contribution of the oxo shell, which then clearly shows this condition has been met (Figure 5). The nodes of the real part of the transform and the shape of the modulus mostly exhibit excellent agreement between the data and the calculation in the region of maximum amplitude where the contribution of the O shell dominates the spectrum over this entire range of Pu–O distances and numbers. A fraction of an O atom at this distance averaged over all of the Pu atoms is a common structural element in all of the different subsets of compounds prepared by different methods. The overlap of the relatively small oxo contribution with those from other shells does increase the error in the calculated numbers of atoms; ratioing analysis gave values 20–30% lower than the curve-fits.

The average Pu–O distance for the compounds precipitated from aqueous solution with ≥ 0.4 oxo atoms is 1.84 Å, ranging from 1.82 to 1.88 Å. The results for the heat-treated materials/precursors, however, show more complicated behavior. The spectra from $PuO_{2.26}$ and $PuO_{2.21}$, the two samples treated at elevated temperature with ≥ 0.5 oxo atoms, give slightly more oxo groups in the fits than the other spectra but exhibit shorter,
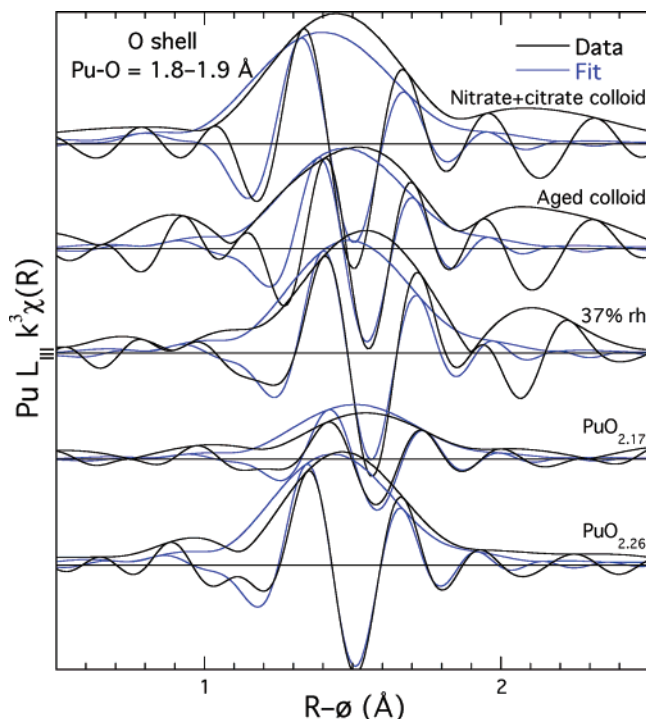
Figure 5. $k^3\chi(R)$, moduli and real parts, of the EXAFS and fits of the spectra from the indicated compounds after subtraction of all shells except the oxo, showing the contribution of the oxo plus background and fit residuals in the measured spectra and the correspondence of this with the oxo shell in the fit.

1.84–1.85 Å Pu–O bonds than the significantly longer, 1.91–1.93 Å Pu–O distances for the other compounds with 0.3–0.4 oxo atom. The average distance for high-fired (b) and the compounds prepared from it by reaction with H_2O is 1.88 Å. Although the errors in the distances may be larger than usual because of the overlap with the contributions from the other shells and the possibility of distortion by background subtraction residuals, the wide range and the clustering for specific sets of compounds suggest the possibility of more than one type of composite oxo bonding mode. This is consistent with the behavior of the peak amplitudes from the near-edge spectral region.

Identification of Valence of Pu Associated with Oxo Groups. Information on the charge distribution—oxo groups occur only for An oxidation states $\geq V$—should be forthcoming from the X-ray near absorption near edge spectra (XANES) region of the XAFS. For Pu, the XANES shifts to higher energy between Pu(III) and Pu(IV) and between Pu(V) and Pu(VI), but its peak decreases in energy and changes shape between Pu(IV) and Pu(V) concomitant with the formation of the highly covalent oxo groups and change in geometry (Figure 6 and Table 2). To first order, the energy of the XANES of Pu(IV/V) mixture could therefore be expected to be close to that of PuO_2, whereas a Pu(IV/VI) mixture would give a spectrum shifted to higher energy by a larger amount for the same number of oxo groups.[11,37] To second order, however, finer aspects of the speciation can modify the spectra by amounts comparable to the valence changes. These can include changes in the shape of the peak that modify its amplitude and therefore produce a

(37) Morris, D. E.; Allen, P. G.; Berg, J. M.; Chisholm-Brause, C. J.; Conradson, S. D.; Donohoe, R. J.; Hess, N. J.; Musgrave, J. A.; Tait, C. D. *Environ. Sci. Technol.* **1996**, *30*, 2322.
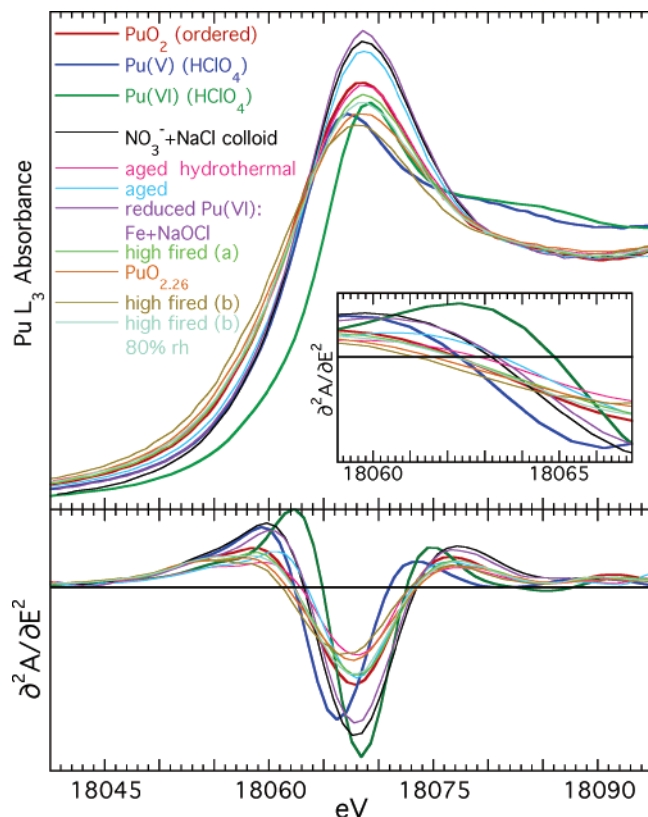
Figure 6. Pu L_III XANES of selected standards and compounds.

better correlation between peak energy and valence than edge energy, so that analysis will use the peak energies instead of the edges as in our original report.[15] A variety of patterns are observed in the XANES of these samples. The peak shift relative to the PuO₂ energy in the spectra from the high-fired (b) set of compounds is -0.1 ± 0.2 eV, whereas the shift from the other high-temperature materials is $+0.6 \pm 0.5$ eV. The shift in the spectra of the precipitated materials is $+0.2 \pm 0.2$ eV, with aging appearing to lower the peak height. In addition to the shifts, the peak amplitudes of the heat-treated materials, including the hydrothermally aged colloid, are all lower than the normalized peak height of 1.55 from PuO₂ by $0.01-0.16$, averaging around 0.1, whereas the peak amplitudes of the precipitated materials are all around 0.15 higher.

The most significant characteristic in assigning the Pu valence from the peak energy is that, although the spectra divide into these groups on the basis of their method of preparation and precursor material, there is no correlation with the putative stoichiometry or the number of oxo groups determined by curve-fits. The peak energy for $x = 0.26$ that gives 0.5 oxo atom in the fits is the same as that for PuO₂, the peak for high-fired (a) with no oxo atoms is 0.2 eV higher, whereas the spectrum from the $x = 0.17$ compound shows the highest shift of all but gives only 0.3 oxo atom in the fits. In contrast, there is a monotonic increase in peak energy with increasing x in the XANES of UO₂₊ₓ.[38] The peak of the isolated spectrum of the Pu–oxo species must therefore coincide in energy with that from PuO₂. This places it roughly halfway between the energies typically found in the XANES of Pu(V) and Pu(VI), indicating that the

actual charge on the Pu is also between these two. In terms of assigning a formal valence, the expanded Pu–oxo bond lengths and the possibility of bridging indicate diminished covalency and therefore decreased donation of the electrons from the oxo ion back to the Pu, resulting in increased charge on the Pu. The Pu bonded to the oxo ions would therefore be Pu(V), although, consistent with the long bond lengths and energy shift, with less covalency than is typical of coordination compounds.

The observed energy and peak shifts must therefore result from other alterations to the structure. In Th(IV) oxyhydroxides, which cannot oxidize above the IV state, the white line decreases in amplitude and possibly in width in association with decreasing $\chi(R)$ amplitudes that signify increasing disorder in both the O and Th shells.[39] We have observed a similar effect in UO₂₊ₓ, which does not show coordination with OH⁻ or H₂O but is forming higher valence U species.[38] Insofar as we prefer to place the ionization energy well down on the absorption edge and therefore assign the peak to the first EXAFS oscillation, lower amplitude would result simply from increased disorder and inhomogeneity. In this EXAFS context, one interesting effect is that the Pu–Pu wave is not in phase with the Pu–O wave that gives the peak, so that, as observed in the heat-treated materials, there is some association between a lower peak in the XANES and a higher Pu peak in $\chi(R)$. Energy shifts would originate in the loss of ligands and the replacement of O²⁻ with other ligands (OH⁻, etc.) that are farther up the posited "spectroscopic series". This leaves the problem that the peak heights from the compounds prepared by aqueous precipitation are not only much higher than those subjected to elevated temperature but also higher than that from ordered PuO₂. The aforementioned correlation with Pu–Pu disorder is one possible contributor to this effect, but is unable to account for all of it. Another possibility from the spectroscopic perspective is that elevating the temperature of the material causes a change in the structure so that the different spectra are indicative of different species. Given that the Pu environments in the two sets of compounds are so similar and that the differences between the $\chi(R)$ spectra and rdf's within the two sets of compounds are larger than the differences between them, there is no structural feature in the one-dimensional representation that can be associated with the change in the spectrum. This leaves as an alternative a change in the three-dimensional structure. Heating may cause a local (but still aperiodic) ordering of the different Pu ligands that results in an alteration of the local stereochemistry. Such changes have been found to shift spectral weight between the L_II and L_III edges in Pt compounds.[40]

Lattice Distortions and Local Speciation in Other PuO₂₍₊ₓ₎ Samples. Since all of these compounds are crystallographically identical except for almost negligible changes in lattice constant and the broadening of the diffraction peaks, one of the more striking aspects of their $\chi(R)$ spectra (Figure 7) is their variability. Although the position of the Pu–Pu peak near $R = 3.7$ Å is almost invariant, its amplitude with k^3-weighting varies by more than a factor of 10. This is the classic type of disordering, in which (semi-)random displacements of the atoms away from their average crystallographic position broaden the distribution and ultimately render it anharmonic. The conserva-

(38) Conradson, S., D.; Clark, D. L.; Lander, G. H.; Manara, D.; Morales, L. A.; Rebizant, J.; Rondinella, V. V.; Wastin, F. *Inorg. Chem.* **2004**, submitted.

(39) Rothe, J.; Denecke, M. A.; Neck, V.; Muller, R.; Kim, J. I. *Inorg. Chem.* **2002**, *41*, 249.
(40) Horsley, J. A. *J. Chem. Phys.* **1982**, *76*, 1451, Conradson, S. D., unpublished results.

Table 2. XANES Parameters: Edge Inflection Point of Ordered Reference PuO_2 = 18062.3 eV Based on First Inflection Point of Zr Metal = 17999.35 eV[a]

sample	edge energy (eV)	ΔeV_e PuO_2	peak energy (eV)	ΔeV_p PuO_2	peak height
Aquo Complexes					
(III) ($HClO_4$)	18060.0	−2.3	18064.3	−4.3	1.85
(IV) ($HClO_4$)	18063.2	0.9	18068.7	0.1	1.72
(V) ($HClO_4$)	18062.3	0.0	18067.6	−1.0	1.43
(VI) ($HClO_4$)	18064.9	2.6	18069.5	0.9	1.47
Hydroxide Ligation					
$PuO_2(OH)_4^2$	18063.9	1.6	18069.3	0.7	1.44
$Pu(VII)O_{2+x}(OH)_y$	18065.4	3.1	18071.5	2.9	1.42
Ordered PuO_2 Reference by Chemical Decomposition					
PuO_2 - cd	18062.3 ± 0.3	reference	18068.6 ± 0.3		1.55
Heat-Treated Samples					
high-fired (a)	18062.2	−0.1	18068.8	0.2	1.50
$x = 0.17$	18063.1	0.8	18069.8	1.2	1.45
$x = 0.26$	18061.6	−0.7	18068.6	0.0	1.43
corroded metal	18062.7	0.4	18069.5	0.9	1.42
$x = 0.21$	18062.4	0.1	18069.2	0.6	1.44
$x = 0.03$	18062.7	0.4	18069.4	0.8	1.47
low-fired	18062.2	−0.1	18068.9	0.3	1.45
high-fired (b)	18061.2	−1.1	18068.2	−0.4	1.39
15% humidity	18062.0	−0.3	18068.6	0.0	1.46
37% humidity	18062.4	0.1	18068.6	0.0	1.53
80% humidity	18062.2	−0.1	18068.7	0.1	1.47
Aqueous Precipitates: Hydrolysis					
nitrate + NaCl	18063.1	0.8	18068.7	0.1	1.69
nitrate	18063.0	0.7	18068.7	0.1	1.70
nitrate + citrate	18063.5	1.2	18068.8	0.2	1.72
aged	18063.4	1.1	18068.6	0.0	1.66
aged hydrothermal	18062.8	0.5	18068.6	0.0	1.54
Aqueous Precipitates: Reduction					
Fe:5 M NaCl	18063.4	1.1	18069.1	0.5	1.70
Fe:5 M NaCl:NaOCl	18063.3	1.0	18068.6	0.0	1.73
Fe:ERDA	18063.1	0.8	18068.7	0.1	1.72
Fe:ERDA:NaOCl	18063.5	1.2	18069.0	0.4	1.70
Al:5 M ERDA	18063.6	1.3	18069.0	0.4	1.71
Al:5 M ERDA:NaOCl	18063.5	1.2	18068.7	0.1	1.71
Substitutional Compounds					
$CaZr_{0.9}Pu_{0.1}Ti_2O_7$	18062.3	0	18068.9	0.3	1.56
$CaZr_{0.4}Pu_{0.6}Ti_2O_7$	18062.0	−0.3	18068.9	0.3	1.50

[a] ΔeV_e PuO_2 = the difference in the energy of the inflection point from that of the PuO_2 spectrum. ΔeV_p PuO_2 = the difference in the energy of the absorption peak from that of the PuO_2 spectrum. Peak height = amplitude of absorption peak normalized as described in Experimental Section.

tion of the X-ray diffraction pattern can therefore be understood as the result of the fact that, even as the high-*Z* Pu sublattice becomes disordered in response to deviations from the perfect PuO_2 stoichiometry and via the addition of H_2O to the compound, the average structure of its coherent fraction remains constant. We have recently found evidence in UO_{2+x} that the coherent and incoherent fractions occur as distinct domains and that the U distribution in the latter is most likely glassy with a total width of several tenths of an angstrom,[38] which suggests that similar processes could be occurring with Pu. In contrast to this single-site Pu distribution with amplitude reduction, the spectral features from the nearest-neighbor O atoms display an enormous range of sizes and shapes up through the base of the Pu peak at $R = 3$ Å, including a splitting of the principal contribution from the crystallographic O shell just below $R = 2$ Å. These features show several preferred locations. The more extended spectral features beyond $R = 4.5$ Å simply diminish in amplitude in parallel with the Pu peak, which is also a typical attribute of increased disorder.

There are also distinct patterns associated with the preparation method. Although there are some extreme cases, such as $PuO_{2.26}$ at the O excess limit, in general the compounds prepared via the high-temperature route have spectra more like the spectrum of PuO_2, with narrower primary O and Pu peaks with much higher amplitudes, fewer and relatively smaller features between $R = 2.4-3.1$ Å, and PuO_2-like features beyond $R = 4$ Å. Poorly diffracting samples prepared by precipitation from aqueous solution display Pu peaks similar or smaller in magnitude as compared to the O peaks, O peaks of reduced amplitude that are significantly broadened or split, and features between these that are large relative to the sizes of these two primary components, and they never show any extended structure past $R = 4$ Å. The more amorphous aspect of the spectra in the precipitated materials is consistent with the larger number of ligand types and greater range of coordination geometries that would be expected from this method of preparation prior to the elimination of water and densification resulting from treatment at high temperature.

The curve-fits corroborate these findings, with the previous admonition that because some of the separations between O shells are near the resolution limit, the general attributes of the resulting radial structure functions (Figure 8) are better depictions of the structure than the literal use of the actual fit results. The Pu—Pu distances in precipitates made by heterogeneous
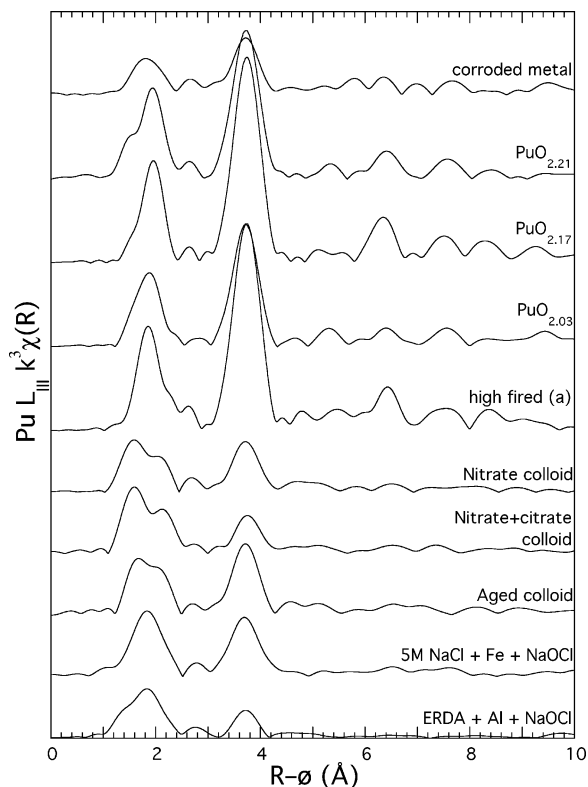
Figure 7. $k^3\chi(R)$ EXAFS moduli of indicated PuO$_2$ species.

Figure 8. Pu partial $g(r)$'s from curve-fitting results of spectra of indicated samples. The Pu shell at 3.8 Å is not weighted by Z but reflects the number of Pu atoms found by the harmonic fit at that location. The vertical lines at 1.86, 2.34, 2.80, 3.06, and 3.32 Å are near where many samples exhibit O shells.

reduction are an average of 0.02 Å shorter, an almost negligible difference that may originate in the anharmonicity of the more disordered Pu distribution. The large errors for the 4.47 Å O shell — despite its 24 atoms, the contribution of this shell to the spectrum is relatively small and it overlaps with that of the Pu — defy attempts to use this shell to identify trends of this type.

The curve-fits distinguish the O shells that overlap in the spectra. From five to as many as eight Pu−O waves at distances of 1.8−3.6 Å are required to fit all of the spectral features associated with the nearest-neighbor O atoms that the crystal structure describes as a single shell. In the 2.6−3.6 Å region, the precipitated compounds all display three O shells with Pu−O distances near 2.8, 3.05, and 3.3 Å. The spectra of most of the high-temperature compounds also show two or three small O shells over this range whose Pu−O distances are close to each other and those of the aqueous precipitates. The similarity in these extra Pu−O distances implies that they originate in Pu coordination with H$_2$O, OH$^-$, etc., that form specific Pu−O(−Pu) moieties that are common among these materials. The nearest-neighbor O shell, corresponding to the one at 2.33 Å in the parent compound, is distinctly broader and often shows extra atomic density both above and below the original distance in the precipitated materials. In contrast, except where maximally disordered (PuO$_{2.26}$), curve-fits of the spectra of the compounds treated at high temperature usually display a peak in the O density close to the crystallographic distance and extra O density predominantly on the low-R side. Their higher, narrower appearance suggests a more ordered structure, consistent with these same attributes for their Pu and 4.7 Å O shells. In addition, when some of these compounds were prepared from the same precursor, the daughters exhibit Pu−O distances closer to the
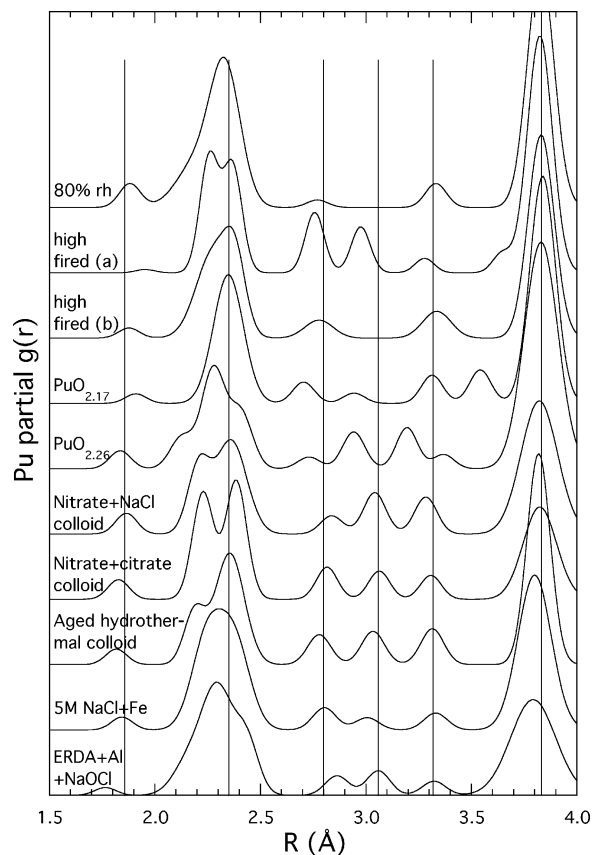
parent material from which they were prepared than to those in other compounds.

Reaction of PuO$_{2+x}$ with H$_2$O under Ambient Conditions. The variety of Pu−O bonds even in fired materials indicates that PuO$_2$ can strongly retain chemisorbed H$_2$O as the same O-containing species found in mononuclear coordination complexes.[11,15] It is therefore of interest to determine if this stability translates into increased reactivity. Consequently, a sample of high-fired oxide was equilibrated with a range of relative humidities under ambient conditions. The resemblance of the spectrum of the starting material to that of PuO$_2$ shows that it was originally highly ordered (Figure 9). The most prominent difference is the distinct shoulder on the low-R side of the O peak. Equilibration with even quite modest amounts of H$_2$O vapor increased the magnitude of both the O and Pu features (also evident in $\chi(k)$) and caused this low-R shoulder to first become resolved and then become larger with higher relative humidities.

The origin of these changes can be tracked in the curve-fit results. The most significant change, paralleling that observed in the original spectra (the increased complexity in the 37rh sample simply recapitulates the behavior of the others in $g(r)$), is the monotonic increase in the number of oxo-type atoms with increasing humidity. This effect was evaluated more closely by subtracting the other Pu−O/Pu waves from the data and comparing the residuals containing the isolated, putative oxo contribution. Although there are some shifts in position and shape, it is nevertheless clear that these features in all four
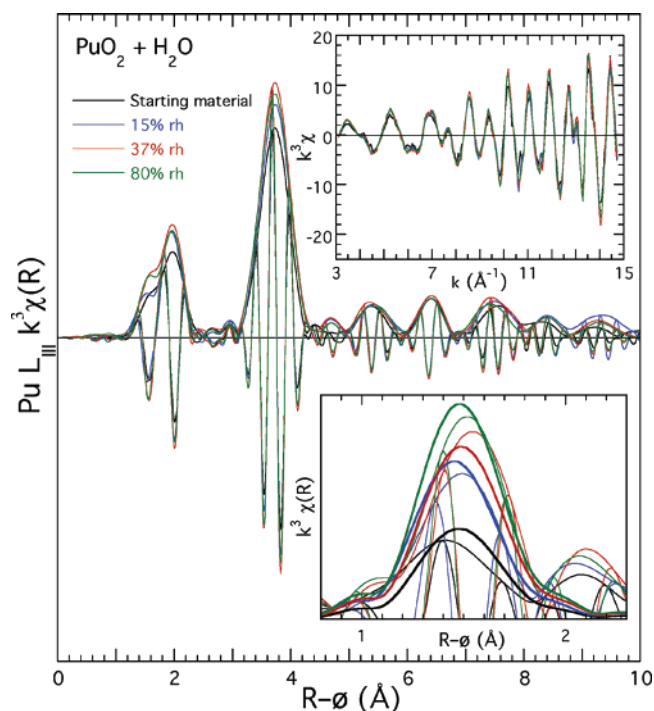
Figure 9. $k^3\chi(R)$ of the EXAFS of PuO_{2+x} high-fired (b) and samples prepared from this compound by reacting with H_2O at different relative humidities at ambient temperature. The modulus and real part of the transform of the data are shown. The insets show the $k^3\chi$ spectra and the moduli and real parts of the isolated oxo contribution and the moduli of the fit to this wave (bold). The vertical scales of the main and $k^3\chi$ plots are identical to those in Figures 1 and 2.

Figure 10. Pu and Zr $k^3\chi(R)$ of the EXAFS of the monoclinic zirconolite, $CaZr_{0.9} \cdot Pu_{0.1}Ti_2O_7$. The modulus and real part of the Pu data and fit are in black and blue, respectively. The modulus of the Zr spectrum, for which the Pu substitutes, is in red. The insets show the Pu $\chi(k)$ data and fit and the moduli of the Pu data, fit, difference, and individual components of the fit (inverted).

spectra are a single peak whose real parts display the same pattern and whose relative magnitudes track the humidity (Figure 9, inset). The correlation of higher number of oxo-type atoms with higher humidities is thus unequivocal in both the spectra and the fit results.

Speciation of Pu(IV) Substituted into Other Oxides. These results raise the question of whether the unexpected behaviors displayed in PuO_{2+x} are unique to the binary oxide or inherent to Pu and therefore more widespread. This was investigated by determining the local structure and speciation of Pu in other oxides. Two examples are the monoclinic zirconolite, $CaZr_{0.9}Pu_{0.1}Ti_2O_7$, and the cubic pyrochlore, $CaZr_{0.4}Pu_{0.6}Ti_2O_7$. The Pu XANES of these compounds (Table 2) exhibit edge energies and absorbance peak intensities at or slightly below and peak energies slightly above those of PuO_2 and therefore closely resemble the spectra of the heat-treated set of PuO_{2+x} materials. The lower symmetry structure of the zirconolite is expected to be more tightly constrained, and the features at $R = 1.0-2.4$ Å in the $\chi(R)$ spectrum (Figure 10) do display a marked resemblance to those in the spectrum of the Zr host for which the Pu substitutes. The cation regions, however, are distinctly different, so that the resemblance of the local environments is limited to the nearest neighbors before preferential substitution and/or lattice distortion affects the more distant shells. The more open and flexible pyrochlore structure shows no similarities between the Pu and Zr spectra and, by implication, speciation and local structure in this compound. This indicates that the Pu is severely distorting the Zr site in which it is believed to reside and in which it is now a majority, modifying it locally into a "Pu" site that does not affect the diffraction pattern because it either retains the average structure or is aperiodic.
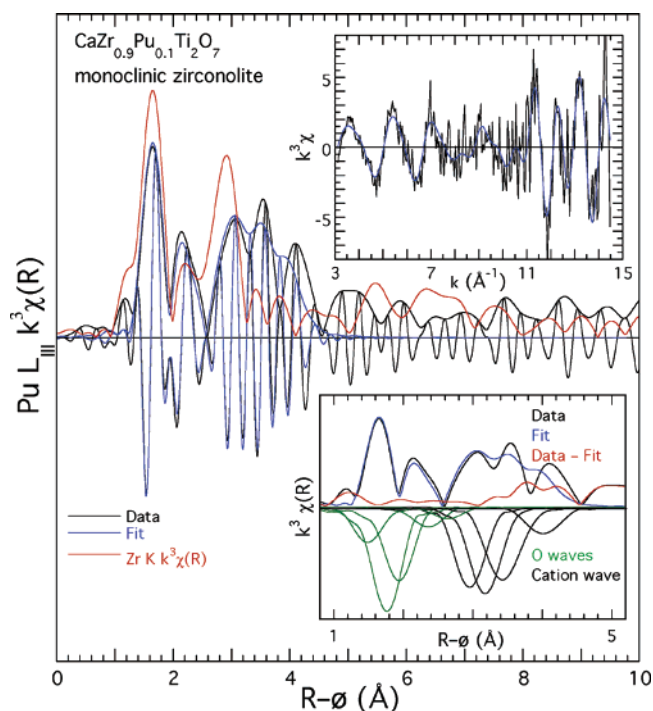
The spectra from both materials require complex O distributions with five shells with Pu–O <3.2 Å to account for most of their features. As with many of the PuO_2 compounds, the reduced amplitude of the primary O shell is best fit with O shells at three overlapping distances with separations that result in substantial destructive interference between their large individual contributions. Both require O shells at very short, oxo-type distances that are well separated from the primary O milieu, and in the pyrochlore spectrum this shell actually fits a resolved feature. The Pu–O component of the rdf's generated from the curve-fits is strikingly similar to those of the disordered PuO_2 compounds. The oxo-type shell and the shells with Pu–O >2.5 Å are very close to those that occur in these PuO_2 samples. The primary O shell also is broad and displays a large component either at or centered near the 2.33 Å Pu–O distance characteristic of PuO_2 as well as substantial atomic density at shorter distances. Insofar as the synthesis of these substituted compounds by high-temperature annealing of anhydrous precursors precludes significant amounts of H_2O and O species derived from it, these findings indicate that within a perturbed oxide lattice the O^{2-} ion and related species can be stabilized at a variety of Pu–O distances, including those observed in disordered PuO_2.

Discussion

The most striking conclusion from this study is that PuO_2 in pure, crystallographic form is rare. Out of 21 independent samples reported here, fully ordered PuO_2 occurred only in those two prepared under strictly anhydrous and mildly reducing conditions. As might be expected, compounds prepared under reducing conditions tend to display fewer, but not necessarily zero, oxo groups, and minimizing exposure to H_2O diminishes

the number of O atoms found at noncrystallographic distances. However, once H$_2$O and its hydrolysis products have been chemisorbed, a process that can be totally separate from the incorporation of excess O and oxidation of the Pu(IV), it is apparently very difficult if not impossible to eliminate from the lattice. This is consistent with recent DFT calculations that indicate that UO$_2$ and PuO$_2$ differ in their affinity for H$_2$O.[41] Similarly, elimination of oxo groups to give homogeneous Pu-(IV) is apparently impeded by solid-state effects; exposure to air is sufficient to partly oxidize at least some materials in this class. It may not, however, be accurate to describe these compounds as disordered. The materials retain some aspects of their long-range average structure and locally are perhaps better portrayed as "differently" ordered. That is, instead of exhibiting the continuous atom densities associated with increasing disorder evolving into glass-like distribution, the distributions continue to exhibit distinct peaks and valleys but at locations in addition to those of the crystallographic structure. The Pu sublattice is retained as the coherent fraction of the Pu structure, and several Pu−O shells clustered around common Pu−O distances are observed. This is evidently a common theme in the cubic AnO$_{2+x}$ family[24,25,39] and probably of even more general application.[42]

Local Coordination Geometry and Collective Effects of the Oxo Groups in PuO$_{2+x-y}$(OH)$_{2y}$·zH$_2$O. In coordination compounds a 1.75−1.80 Å Pu−O distance constitutes a Pu-(VI) trans-dioxo moiety, while Pu(V)−oxo distances are 0.03−0.05 Å longer (both expanded 0.03−0.05 Å with OH/R$^-$ equatorial ligands). The long distances and XANES energies found here support the assignment of the excess charge to Pu-(V) rather than the Pu(VI) state, albeit Pu(V) that is more highly charged than usual. The Pu(IV):Pu(V) ratio for $x = 0.25$ is 1:1, so that if the Pu(V) were in the normal dioxo configuration, one oxo atom per Pu would be expected. Of course, these stoichiometries are not based on direct measurement but inferred from H$_2$ evolution during the reaction. The high-fired (a) starting material did not show any oxo groups but did show substantial numbers of O atoms at other noncrystallographic positions, so the actual O excess and its disposition after reaction at elevated temperature are ambiguous. PuO$_{2.03}$ apparently has a much higher amount of excess O, so that its starting material must have also had more O than expected (possibly as H$_2$O and not Pu(V)−oxo). The plateau in the H$_2$ evolution during the reaction was evidently not the conjectured PuO$_{2.00}$. Inferring stoichiometry from H$_2$ evolution, even in combination with diffraction measurements, may not be an ideal method for determining x. A further complication would ensue if the excess O sites act cooperatively to form stable clusters and domains that would enable two or more distinct species to coexist in the crystal, as has been postulated for the analogous UO$_2$ system.[23] Since, as in UO$_{2+x}$, the different structures do not give separate diffraction patterns, these domains must be below the diffraction limit in size and therefore intimately associated with each other as well as being aperiodically arranged.[19,43] U and Np also demonstrate

that oxo configurations and geometries that do not occur in solution − symmetric actinate, mono-oxo, bent dioxo, tetraoxo, etc. − are found in solids. Utilizing only moieties with precedents in coordination chemistry may not be an adequate basis for deducing the local speciation and local and extended structure. O ligands in solution and molecular complexes are isolated from the medium or at most bridge two Pu ions, whereas here they are automatically surrounded by large numbers of atoms at very short distances.

The O-incorporation mechanism must account for how not only these oxo groups but also the entire Pu(V) sites with which they are associated are situated within the materials. Another factor, in addition to the Pu geometry shift to a (bi-)pyramidal or related conformation, is that valences greater than or equal to V are associated with coordination numbers less than those found with Pu(IV). The excess O atoms must therefore be added so that the O atoms already present are displaced to positions that split them off from some of their Pu neighbors. This is a characteristic of the proposed defect clusters in UO$_{2+x}$, which use the octahedral holes as centers on a defect chain along [001] for rotating a pre-existing and a new O atom by 90° in a (110) plane and then shifting them toward the hole along [110] to reduce their overlap with their neighbors, leaving the U atoms in their original positions.[24] The problem with this model is that it distributes the increased charge over many U atoms by small reductions in U−O distances with retention of eight O nearest neighbors and an increase to nine for the two U atoms at the ends of the chain. By reinforcing spherical types of geometries with large numbers of neighbors, it inhibits the formation of oxo groups and the associated normal plane of the pyramid that contains the equatorial ligands.

The constraints on the arrangements of the atoms can be explored through simple combinations utilizing the crystal symmetries and the fact that the Pu atoms should remain on or close to their original positions (Figure 11). Placing oxo atoms along ⟨100⟩ vectors toward the octahedral holes actually causes the most problems because of the subsequent difficulty in arranging the other atoms of the O$_8$ cube into a normal plane through the Pu. A square bipyramid around a Pu site is formed trivially from the four O neighbors in the (101) plane two O atoms at 0 $\frac{1}{2}$ 1 and 1 $\frac{1}{2}$ 0 on the edge centers on vectors normal to this plane (setting aside the issue of the other two or four O atoms at the vertices of the O$_8$ cube that are not included). These new O atoms then bridge the original Pu and its two neighbors along the same vectors at 1.9 Å Pu−O distances, similar to an asymmetric actinate. The oxo atoms can also be along ⟨111⟩ vectors. Displacement of the O atoms at these vertices of the O$_8$ cube by 0.42 Å to give a Pu−O distance of 1.9 Å only elongates the Pu−O distances to the other three Pu ions that formed the base of the Pu tetrahedron around these O atoms to 2.40 Å, which is easily within the primary O shell distribution. Rotating the central bipyramid to tip the oxo ion off of the 3-fold rotation axis of the Pu tetrahedron would then give two bonds around 2.2 Å and one bond around 2.8 Å, again consistent with the experimental results. In this case, the bipyramidal geometry would be completed by having some of the O^{2-} ions from the other six vertices become equatorial ligands in the (111) plane. This would necessitate displacements within their Pu tetrahedra with a 0.29 Å component parallel to the oxo vector so as to reside in the equatorial plane. Since if the displacement were

(41) Martin, R. L.; Hay, P. J. personal communication.
(42) Welberry, T. R.; Withers, R. L.; Mayo, S. C. *J. Solid State Chem.* **1995**, *115*, 43. Argyriou, D. N.; Elcombe, M. M. *J. Phys. Chem. Solids* **1996**, *57*, 343.
(43) Conradson, S. D.; Espinosa-Faller, F. J.; Villella, P. M. In *11th International Conference on X-ray Absorption Fine Structure (XAFS XI)*; Munksgaard International Publications Ltd.: Ako, Japan, 2001; Vol. 8, p 273.
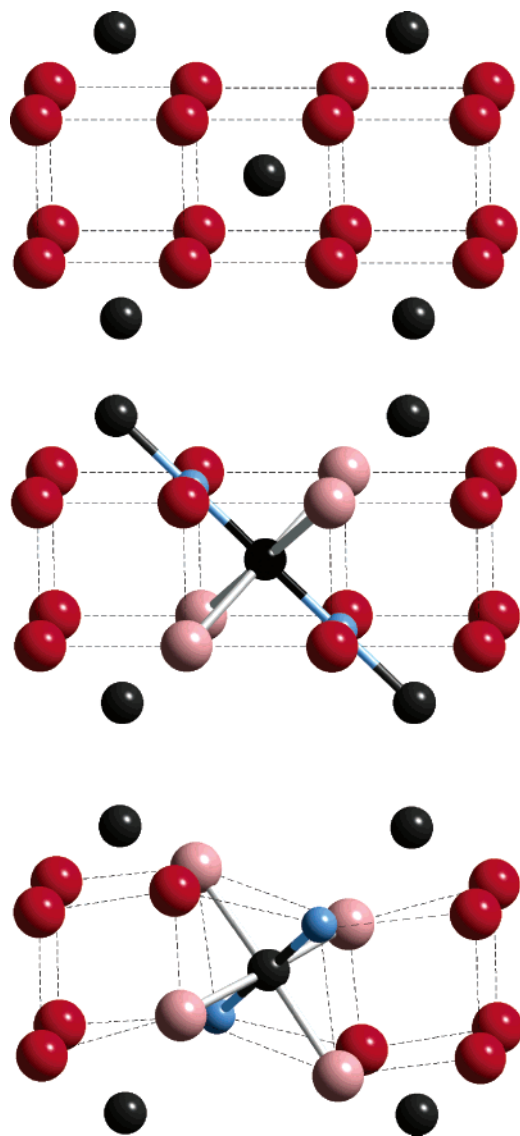
Figure 11. Schematic mechanisms for incorporation of trans-dioxo Pu(V) moiety into cubic Pu(IV) site in PuO$_2$ (top). Pu(IV) ions are black, O^{2-} ions red, the Pu(V) is gold, oxo ions are blue, and the O ions coordinated to the Pu(V) that reside in the plane normal to the O=Pu=O axis are pink. Bonds from the Pu to the latter two types of O are shown, and the framework of the O sublattice is indicated with dashed lines. The middle picture shows the addition of two oxo groups with Pu–O = 1.9 Å normal to a (110) plane of the PuO$_8$ cube. In this case the four equatorial ligands are already in place. The oxo groups are inserted between the O^{2-} ions at the vertices of the PuO$_8$ cube that are not involved in the equatorial coordination, giving 1.35 Å O–O distances. Since these oxo groups are midway between two Pu ions, they automatically form the same type of bond to the Pu ion in the diagonally adjacent cell. The lower picture shows the conversion of two of the O^{2-} ions at opposite vertices of the PuO$_8$ cube into oxo groups so that the O=Pu=O vector is normal to a [111] plane through the cube. In this case they are displaced toward the central Pu(V), avoiding the problems of bridging to neighboring Pu ions and overlapping with other O ions. However, four of the O^{2-} ions from the other vertices must be displaced into the (111) plane to create a set of equatorial ligands, and the other two were displaced toward the adjacent cation holes. Although these Pu–O bonds are long, these displacements also create additional Pu–O distances <1.9 Å asymmetrically with neighboring Pu ions.

constrained to only ⟨111⟩ vectors this would give 2.05 Å O–O distances, there must be components in other directions. Additional simple displacements of the O atoms within the equatorial plane split these distances to give 1.85 and 2.25 Å Pu–O separations.

On the basis of strictly geometrical considerations, it is therefore not necessarily difficult to insert oxo ions into the PuO$_2$ lattice to create a trans-dioxo Pu(V) site that retains the Pu positions and gives the experimental Pu–O distances. Further easing of the spatial constraints would be facilitated by rotating the most obstructive O atoms toward the octahedral holes, and the XANES has already suggested the possibility of multiple conformations. What cannot be easily — or perhaps at all — accomplished is doing this in such a way that additional short, Pu–oxo-type bonds are not automatically created at the neighboring sites. The [111] displacement results in one 1.90 Å and three 2.40 Å Pu–O distances (or one 1.90 Å, two 2.20 Å, and one long distance with concomitant rotation). This implies that Pu(V) sites are coupled via O displacements in one cell that create Pu–oxo bonds in neighboring cells, forming extended O-defect clusters.

Local Coordination Geometry and Collective Effects of Other Pu–O Species in PuO$_{2+x-y}$(OH)$_{2y}$·zH$_2$O. In addition to the 1.8–1.9 Å Pu–O distances just discussed, the noncrystallographic Pu–O distances that often occur are sufficiently short to be considered as overlapping, bonded atoms similar to those found in coordination complexes involving other O-based ligands: Pu–OH$^-$ at 2.2–2.3 Å, Pu–O^{2-} (four Pu neighbors) at 2.33 Å, Pu–OH$_2$ at 2.4–2.5 Å, etc. These involve coordination with H$_2$O or H$_2$O-hydrolysis products (OH$^-$) and subsequent charge balancing via creation of Pu vacancies or H$^+$ substitution. The description as PuO$_{2-y}$(OH)$_{2y}$·z(H$_2$O) is analogous to the ThO$_2$ system, which cannot have higher valent Th.[39] The addition or substitution of these other ligands for the normal O^{2-} will induce distortions as the Pu–O pair attempts to attain a separation that is more normal for each particular species and as neighboring ions are displaced to accommodate their larger sizes and irregular shapes. The presence of these distances and implied speciation in materials prepared from or reacted with H$_2$O suggests that these PuO$_2$-derivative compounds are in explicit chemical equilibrium with H$_2$O involving hydrolysis, addition, and substitution as well as oxidation and diffusion. Although treatment at high temperature sharpens the distributions and, by inference, anneals the material, even at the highest temperatures it does not necessarily result in the elimination of H$_2$O and the formation of pure, ordered PuO$_2$. Nevertheless, the XANES shows that heating probably induces a specific modification to the local structure. The H$_2$O-hydrolysis adducts apparently are sufficiently stable within the lattice, even if they do not form an ordered phase, that they defeat the normal preference for the homogeneous, ordered, crystalline material. This may be significant in terms of the expectation that the solubility of species identified in the solid will track that of pure phases or mononuclear, molecular coordination complexes. Recent DFT calculations indicate that chemisorbed H$_2$O is more stable in PuO$_2$ than in UO$_2$, which is consistent with these results.[41] Another essential aspect of the direct coordination of H$_2$O and related species without oxidation is that is appears to be very much independent of the oxidation process but is at least somewhat associated with Pu–Pu disorder. Some samples with larger numbers of oxo groups show a high degree of Pu–Pu ordering and relatively few atoms with Pu–O distances between 2.4 and 3.5 Å, analogous to UO$_{2+x}$.[38] Other samples with small Pu–Pu contributions and large numbers of O atoms

at noncrystallographic distances have negligible numbers of oxo atoms, analogous to the Th(IV) oxyhydroxide colloid system.[39]

Chemical Basis for Oxidation. The conundrum for PuO$_{2+x}$ has always been that, unlike U and Np, the lack of binary oxides with valence greater than IV defies traditional thermodynamic and crystallographic logic because the higher valence Pu species then exist only as a fraction of the Pu within the PuO$_2$ lattice, which they render inhomogeneous. Furthermore, the energy lost through destabilizing the lattice is exacerbated by the fundamental energetics of Pu. The potential for the oxidation of mononuclear Pu(IV) $\rightarrow$ Pu(V) in solution is 1.04 V (cf. 0.99 V for Pu(IV) $\rightarrow$ Pu(VI) and 0.94 V for Pu(V) $\rightarrow$ Pu(VI)), 0.6 V at pH 8, and drops to 0 only at pH 14 with excess CO$_3^{2-}$.[5] Calculations indicate that the actual charge of O^{2-} in PuO$_2$ and, by extension, its alkalinity in PuO$_2$ are typical of metal oxides, so that Pu(V) is not unusually stabilized in the solid.[41,44] PuO$_2$ has therefore been considered the thermodynamic well in the Pu$-$H$_2$O system. Given the conceptual barriers, it was then incumbent upon those proposing PuO$_{2+x}$ to provide unequivocal evidence for its existence. Such evidence was not easily forthcoming until the combined sequence of controlled preparation and crystallography[3] because the Pu(V) photoemission signal and other experimental signatures are not easily resolved in the inhomogeneous material.[7,8,45] These XAFS results demonstrate that this "destabilized", inhomogeneous lattice is the preferred form not only with respect to the facile oxidation of up to half of the Pu to Pu(V) with its awkward oxo geometry but also for chemisorbed H$_2$O. An important corollary to this is that, since the inhomogeneous materials are apparently more stable than pure PuO$_2$, the conjecture that the Pu(V) component of PuO$_{2+x}$ might be leached out because of the higher (molecular) solubility of Pu(V) does not appear correct.

Understanding this phenomenon first requires accepting that the energetics given by electronic structure calculations can be far from a complete description of a system. A second critical aspect is that these distortions must propagate collectively through the cubic structure. Any displacement, addition, or modification of an O moiety affects the Pu local structure and speciation in all of the unit cells that share it. It may therefore require very large numbers of atoms to calculate a reasonably accurate energy value. The propagation that ultimately must produce a large degree of cooperative behavior in the structure naturally extends to the idea of nanoscale heterogeneity.[19,43,46] The development of UO$_{2+x}$ incorporates this idea, that the defects cluster to form ordered domains that anticipate and eventually grow into the next phase.[23,24] In general, local composition fluctuations resulting from random or locally ordered distributions of atoms, possibly enhanced by cooperative effects between the distorted sites, will cause the atoms in these regions to rearrange to form domains with a different but still ordered structure. This second structure will be highly constrained by the necessity of conserving the density to minimize total elastic strain and also minimizing epitaxial mismatch and interfacial strain, which is assisted by the small length scale. Such domains can easily occupy >20% of a crystal without giving a unique signal in the diffraction pattern since they are below the diffraction limit in size and can be arranged in aperiodic, incoherent ways, such as filamentary or randomly sized and shaped globular structures.[19,46] Countering losses of crystal and electronic energy, the essential thermodynamic factor is the finite temperature, total free energy that will be lowered by two-state entropy contributions, and Ginsburg$-$Landau-like fluctuations in the order parameter describing the conversion between these states. These rules dictating the morphology of the extended structure and the mechanisms by which the total free energy is decreased mean that the second structure may not exist as a separate entity: it may only occur in the solid state in intimate association with and as the result of cooperative effects with the host.[11] For the PuO$_{2+x-y}$(OH)$_{2y}$·zH$_2$O system, the density is preserved by maintaining the Pu sublattice, the formation of large ordered domains is inhibited by the asymmetry of oxo group addition and H$_2$O-derived substitution across the unit cell faces, and the order parameter is the chemical extent of Pu(IV) oxidation or substitution rather than a phase transition.

The conceptual distinction between cooperativity-controlled heterogeneity and homogeneity not only is evident in the structure but also offers an explanation for the reactivity and thermodynamics. The oxidation of UO$_2$ proceeds continuously and homogeneously to the known U$_4$O$_9$ and U$_3$O$_7$ phases (and then beyond), with the O added prior to phase transformation forming domains analogous to the U$_4$O$_9$ structure.[24,25] Since there are, however, no crystallographically distinct Pu$_4$O$_9$ or higher valence Pu$_2$O$_5$ or PuO$_3$ compounds or structures, the oxidation of Pu stops with the material still in the PuO$_2$ phase. This difference between the binary Th/U/Np and Pu(IV) oxides will then originate in the fact that some PuO$_{2-y}$(OH)$_{2y}$·z(H$_2$O) sites or domains in PuO$_{2+x}$ will undergo facile addition of oxo groups, whereas the elastic strain involved in their incorporation into the lattice will cost energy for others. The ease of the oxidation will vary, so that some sites may add O under very mild conditions and others will require higher temperatures and pressures. Using a plateau in H$_2$ evolution as a signature of PuO$_{2.00}$ thus resulted in the unexpected formation of a compound with a much larger number of oxo groups than expected for the conjectured $x = 0.03$. The reaction then saturates at $x = 0.25$ without crystallographic order that would allow it to continue through other phases. Thermodynamic extrapolations based on a homogeneous model[9] are therefore incomplete and will fail to adequately describe all of the observed behaviors.

This model using nanoscale heterogeneity has implications beyond the immediate results. It corroborates the atomic-scale mechanism for the ripening of precipitates as a low-density form with vacancies and a higher susceptibility for inclusions transforms to a higher density one with more bridging and fewer terminal ligands that will be less soluble. It also implies, however, that the ripening process may not converge to a single value or be irreversible, so that the use of a single value for the solubility constant may be an extreme oversimplification. The finding of multiple types of PuO$_2$ also provides an explanation for the enormous variability in corrosion initiation and rates affecting the metal. This in turn suggests that the promotion of certain characteristics in the surface oxide by specific treatments of the metal surface could produce much more consistent corrosion properties. Similarly, the use of local structure and speciation as a specification in the preparation of PuO$_2$ could enhance its reliability as a long-term storage form.

(44) Wu, X. Y.; Ray, A. K. *Phys. Rev. B: Condens. Matter* **2002**, *6508*, 5403.
(45) Haire, R. G.; Haschke, J. M. *MRS Bull.* **2001**, *26*, 689.
(46) Conradson, S. D.; Espinosa-Faller, F. J.; Henderson, A.; Villella, P. M. In *International Symposium on Physics in Local Lattice Distortions (LLD2K)*; Oyanagi, H., Bianconi, A., Eds.; American Institute of Physics: Ibaraki, Japan, 2000; Vol. 554, p 503.

Finally, it is highly unlikely that PuO_2 is the only metal oxide that displays these behaviors. The possibility of nanoscale heterogeneity and its effect on the chemistry of mixed-valence metal oxides should be considered to the same extent as charge-ordering and its effect on physical properties.

Note Added in Proof. While this manuscript was in proof, a publication appeared that examined EXAFS data on aqueous Pu(IV) colloids (Rothe, J.; Walther, C.; Denecke, M. A.; Fanghanel, Th. *Inorg. Chem.* **2004**, *43*, 4708). These authors also found indications of short Pu—O distances less than 2 Å in their EXAFS data. They argued that a Pu—O < 2 Å was not physically meaningful for a Pu(IV)—O bond and suggested that this feature arises due to multielectron excitation. In our work, the isolation of $PuO_{2.26}$ was key to the determination that Pu(V) is present in these PuO_{2+x} materials and that a Pu(V)—O distance of 1.8−1.9 Å is not only physically reasonable but also very common in PuO_{2+} ions. This recognition allowed us to determine that this spectral feature originates from a Pu(V)—O unit in both PuO_{2+x} solids and in precipitated Pu(IV) colloids that must necessarily be partially oxidized, as discussed in the text.

Supporting Information Available: Three-part figures as in Figure 2 for all samples, comparisons of spectra as in Figures 6 and 7, and distribution functions as in Figure 8 that include more samples. This material is available free of charge via the Internet at http://pubs.acs.org.

JA049192E